

Diffuse emission of high-energy neutrinos from gamma-ray burst fireballs

Irene Tamborra^a and Shin'ichiro Ando^a

^aGRAPPA Institute, University of Amsterdam, Science Park 904, 1098 XH, Amsterdam, The Netherlands

E-mail: i.tamborra@uva.nl, s.ando@uva.nl

Abstract. Gamma-ray bursts (GRBs) have been suggested as possible sources of the high-energy neutrino flux recently detected by the IceCube telescope. We revisit the fireball emission model and elaborate an analytical prescription to estimate the high-energy neutrino prompt emission from pion and kaon decays, assuming that the leading mechanism for the neutrino production is lepto-hadronic. To this purpose, we include hadronic, radiative and adiabatic cooling effects and discuss their relevance for long- (including high- and low-luminosity) and short-duration GRBs. The expected diffuse neutrino background is derived, by requiring that the GRB high-energy neutrino counterparts follow up-to-date gamma-ray luminosity functions and redshift evolutions of the long and short GRBs. Although dedicated stacking searches have been unsuccessful up to now, we find that GRBs could contribute up to a few % to the observed IceCube high-energy neutrino flux for sub-PeV energies, assuming that the latter has a diffuse origin. Gamma-ray bursts, especially low-luminosity ones, could however be the main sources of the IceCube high-energy neutrino flux in the PeV range. While high-luminosity and low-luminosity GRBs have comparable intensities, the contribution from the short-duration component is significantly smaller. Our findings confirm the most-recent IceCube results on the GRB searches and suggest that larger exposure is mandatory to detect high-energy neutrinos from high-luminosity GRBs in the near future.

Contents

1	Introduction	1
2	Observational constraints on gamma-ray bursts	2
2.1	Long duration gamma-ray bursts	3
2.2	Short-duration gamma-ray bursts	5
3	Prompt neutrino emission from gamma-ray burst fireballs	6
3.1	Neutrino production from pion decay	7
3.2	Neutrino production from kaon decay	10
3.3	Neutrino energy spectra	13
3.4	Neutrino flavor oscillations	15
4	High-energy diffuse neutrino background from gamma-ray bursts	17
4.1	Expected diffuse background and uncertainties on the local rate and luminosity function of each GRB family	17
4.2	Expected diffuse background and uncertainties on the jet parameters	19
5	Discussion and conclusions	21

1 Introduction

Gamma-ray bursts (GRBs) are among the most energetic events in the Universe (see e.g. [1, 2] for reviews on the topic) and have been suggested as sources of ultra-high energy cosmic rays [3, 4]. In terms of astronomical observations, they are usually divided into two distinct groups on the basis of the BATSE bimodal distribution: Long-duration bursts (whose duration is longer than 2 s) and short-duration bursts (lasting for less than 2 s) [5]. Long duration bursts are thought to originate from the collapse of a massive star to a black hole [6], while short-duration ones should originate from coalescing neutron stars or black-hole–neutron-star mergings [7].

It is not excluded that, although with different origin, short- and long-duration bursts are driven by the same underlying mechanism: The fireball model [8–10]. According to this model, a hot “fireball” of electrons, protons and photons forms. Such fireball is initially opaque to radiation, then the hot plasma expands by radiation pressure and particles are accelerated making the plasma transparent to radiation and favoring the emission of keV–MeV photons [11, 12]. Neutrinos with energies of $\mathcal{O}(100)$ TeV are also expected to be emitted from these sources because of lepto-hadronic interactions [8]. Besides the fireball emission model [8, 10] on which we will rely in this work, other models have been proposed to explain the neutrino production in GRBs, such as the dissipative photosphere model [13] according to which the prompt GRB emission occurs near the Thomson scattering photosphere, or large-radius magnetic dissipation models, such as the ICMART model that relies on a highly magnetised outflow which is dissipated at a radius larger than the internal shock radius [14]. See [15] for a common formalism to connect these models and a comparison among the expected neutrino fluxes.

The IceCube detector, a neutrino telescope made with 5160 optical modules and located at the South Pole, could detect neutrinos from GRBs by measuring the Cherenkov light from secondary particles produced in the neutrino-nucleon interactions. Over the past years, IceCube performed searches for muon neutrinos associated to GRBs, but with negative results [16–20]. The IceCube upper limits therefore started to put tight constraints on the expected GRB flux and on the theoretical models employed to explain the neutrino emission from these sources [21, 22]. The diffuse neutrino emission from GRBs is also widely discussed in the literature [23–31] and it has been recently invoked [32–39] as a natural possibility to explain the PeV neutrino events discovered from IceCube [40–43], assuming such events have a diffuse origin (see [44] for an overview on the possible astrophysical sources of the IceCube PeV neutrinos and references therein).

In light of the unsuccessful most recent IceCube stacking analysis [43] and of the high-energy neutrino flux discovery [40–43], the aim of this work is to provide an up-to-date estimation of the expected high-energy neutrino prompt emission from long- and short-duration GRB families within the fireball model [9, 10]. To this purpose, for the first time we present an analytically extensive modelling of the neutrino emission from fireballs by including radiative, adiabatic and hadronic cooling processes involving pion and kaon decays. Then, we discuss the relevant processes for each GRB family (high-luminosity, low-luminosity and short GRBs) and derive an estimation of the diffuse flux by adopting up-to-date gamma-ray luminosity functions and evolution of formation rates to fix the normalization of the GRB neutrino energy spectrum.

Our results show that, for average GRB parameters compatible with observations, the diffuse neutrino emission from GRBs could contribute up to a few % to the currently observed IceCube high-energy neutrino flux in the sub-PeV region while GRBs might be the main source of the IceCube flux in the PeV range, assuming that the latter has a diffuse origin. Moreover, we find that the neutrino emission within the fireball model is widely compatible with the current IceCube limits due to stacked GRBs.

This manuscript is organised as follows. In Section 2 we introduce constraints coming from gamma-ray observations on the luminosity functions and redshift distribution of long-duration (divided in low-luminosity and high-luminosity GRBs) and short-duration GRBs. In Sec. 3, we analytically model the neutrino emission from $p\gamma$ interactions in GRBs and define the expected neutrino spectrum from pion and kaon decays including radiative, adiabatic and hadronic cooling processes. In Sec. 4, we present our results on the diffuse emission from these sources, discussing the astrophysical uncertainties as well as the ones related to the GRB model parameters, and compare them with IceCube bounds and future searches. Conclusions are presented in Sec. 5.

2 Observational constraints on gamma-ray bursts

Gamma-ray bursts have been monitored since long time now. They are usually divided into two families according to the observation of these transients in photons: Long- and short-duration bursts. However, current data are still insufficient to define accurate luminosity functions, especially at high redshifts. Sources of errors are, for example, the triggering criteria of the detection instruments that can be responsible for poor estimates in the parameters, degeneracies arising from a mixing of the luminosity function and the source rate evolution with the redshift, as well as selection effects. Given such uncertainties, in the following we will define allowed bands for the distribution of the GRB families in luminosity and redshift

Table 1. GRB parameters adopted in the estimation of the diffuse high-energy neutrino flux for our *canonical* model including the astrophysical uncertainties. The local rate (ρ_0) is in units of $\text{Gpc}^{-3} \text{ yr}^{-1}$, the isotropic luminosities (\tilde{L}_* , \tilde{L}_{\min} and \tilde{L}_{\max}) are expressed in units of $10^{52} \text{ erg s}^{-1}$, the variability time t_v is in s. The best fit parameters α and β are employed in the luminosity function fits, while α_γ and β_γ describe the gamma-ray Band spectrum, and Γ is the bulk Lorentz factor of the jet.

	ρ_0	\tilde{L}_*	α	β	\tilde{L}_{\min}	\tilde{L}_{\max}	α_γ	β_γ	Γ	t_v
HL-GRB	0.8	0.8	-0.95	-2.59	10^{-3}	10^2	1	2	500	0.1
HL-GRB	0.5	0.48	-0.13	-2.42	10^{-3}	10^2	1	2	500	0.1
LL-GRB	2000	5×10^{-4}	-2.3	-1.27	1.8×10^{-6}	10^{-3}	1	2	5	100
LL-GRB	200	5×10^{-4}	-2.3	-1.27	1.8×10^{-6}	10^{-3}	1	2	5	100
sGRB	$4.6^{+1.9}_{-1.7}$	2	-1.94	-3.0	0.5×10^{-3}	10	0.5	2.25	650	0.01

and characterize the source energetics. Unless otherwise specified, we will distinguish among three different reference frames: The GRB reference frame, the jet comoving frame and the observer frame. Each physical quantity X will be labelled as \tilde{X} , X' , and X in each of these frames respectively.

2.1 Long duration gamma-ray bursts

Long-duration GRBs are thought to originate from the collapse of a massive star into a black hole [6]. They are usually divided in two sub-categories: High-luminosity (HL) and low-luminosity (LL) GRBs.

The source rate evolution as a function of the redshift (z) of the HL component is described through a piecewise function [45]:

$$R_{\text{HL-GRB}} = \rho_0 \begin{cases} (1+z)^a & \text{for } z < z_* \\ (1+z_*)^{a-b}(1+z)^b & \text{for } z \geq z_* \end{cases}, \quad (2.1)$$

being ρ_0 the local rate defined as in Table 1, $z_* = 3.6$, $a = 2.1$, and $b = -0.7$ [46].

The HL-GRB typical luminosities vary in the range $[10^{49}, 10^{54}] \text{ erg s}^{-1}$. We adopt the intrinsic isotropic luminosity function (LF), i.e., corrected for beaming effects and defined in the GRB frame, found in [47] on the basis of a selected sample of 175 bursts observed by *Swift*:

$$\Phi_{\text{HL-GRB}} \propto \begin{cases} \left(\frac{\tilde{L}_{\text{iso}}}{\tilde{L}_*}\right)^\alpha & \text{for } \tilde{L}_{\text{iso}} < \tilde{L}_* \\ \left(\frac{\tilde{L}_{\text{iso}}}{\tilde{L}_*}\right)^\beta & \text{for } \tilde{L}_{\text{iso}} \geq \tilde{L}_* \end{cases}, \quad (2.2)$$

with best-fit parameters defined in Table 1 [47]. Note that in Table 1 we consider two sets for the LF parameters and for the local rate ρ_0 , corresponding to the extremes of the accepted band allowed from the data (see [47] for more details). Figure 1 shows the redshift distribution of the HL-GRB family in light blue. The uncertainty band is defined by the two extreme sets of parameters in Table 1 for HL-GRBs. The distribution of these sources peaks at about $z \simeq z_*$ and it stays roughly constant at higher redshifts.

The LL-GRBs are characterised by isotropic equivalent luminosity much smaller than that of the HL-GRBs, i.e. 10^{46} – 10^{49} erg s $^{-1}$. The origin of the LL component is not yet clear. It is not excluded that the LL-GRBs belong to a distinct population than the HL-GRBs [48]. On the other hand, it could be that they have the same origin as HL-GRBs, but are produced by failed jets that do not break out of their progenitors. According to the latter hypothesis, this could mean that most supernovae generate jets producing LL-GRBs and only few of them are able to produce jets powerful enough to break out and produce HL-GRBs [49]. Due to their low-luminosity, LL-GRBs have been mainly detected nearby ($z \leq 0.1$) and a large fraction of their population might be below the detection threshold.

In order to estimate the LL-GRB total event rate, we assume a supernova–GRB connection, and suppose that the LL-GRB rate should be lower than the one of type Ib/c supernovae. Therefore, we define the LL-GRB rate as [23, 50]:

$$R_{\text{LL-GRB}} = \rho_0 \left[(1+z)^{p_1\kappa} + \left(\frac{1+z}{5000} \right)^{p_2\kappa} + \left(\frac{1+z}{9} \right)^{p_3\kappa} \right]^{1/\kappa}, \quad (2.3)$$

with $\kappa = -10$, $p_1 = 3.4$, $p_2 = -0.3$, $p_3 = -3.5$, and we consider two representative values for the fraction of SN Ib/c that goes in LL-GRBs [23], i.e., $\rho_0 = 0.01 \rho_{\text{SN}}$ and $\rho_0 = 0.1 \rho_{\text{SN}}$ with $\rho_{\text{SN}} = 2 \times 10^4 \text{ Gpc}^{-3} \text{ yr}^{-1}$ [51]. The LL-GRB rate is shown as a function of the redshift in Fig. 1 (violet band), it peaks at $z \simeq 1$ and it decreases at higher redshifts. Note that it is locally much higher than the HL-GRB one.

The LL-GRB LF is parametrized as in [23, 52]:

$$\Phi_{\text{LL-GRB}} \propto \left[\left(\frac{\tilde{L}_{\text{iso}}}{\tilde{L}_*} \right)^\alpha + \left(\frac{\tilde{L}_{\text{iso}}}{\tilde{L}_*} \right)^\beta \right], \quad (2.4)$$

with \tilde{L}_* , α and β as in Table 1 based on the *Swift*-BAT sample analysed in [52]. Although the adopted LF fit describes both the LL and HL-GRBs [52], we use it for the LL-GRB component only.

For both the LL- and HL-GRBs, we assume that the injected (inj) gamma-ray energy spectrum is fitted with a Band-spectrum [53]:

$$\left(\frac{dN_\gamma}{dE'_\gamma} \right)_{\text{inj}} \propto \begin{cases} \left(\frac{E'_\gamma}{E'_{\gamma,b}} \right)^{\alpha_\gamma} & \text{for } E'_\gamma < E'_{\gamma,b} , \\ \left(\frac{E'_\gamma}{E'_{\gamma,b}} \right)^{\beta_\gamma} & \text{for } E'_\gamma \geq E'_{\gamma,b} , \end{cases} \quad (2.5)$$

with $\alpha_\gamma = 1$ and $\beta_\gamma = 2$ as in Table 1. The photon break energy $E_{\gamma,b}$ is usually expressed as a function of the isotropic energy (E_{iso}) through the so-called ‘‘Amati relation’’ that holds for the long-duration GRBs [54, 55]:

$$\frac{\tilde{E}_{\gamma,b}}{0.1 \text{ MeV}} = (3.64 \pm 0.04) \left(\frac{\tilde{E}_{\text{iso}}}{7.9 \times 10^{52} \text{ erg}} \right)^{0.51 \pm 0.01}. \quad (2.6)$$

The isotropic energy of each GRB in the source rest frame can be expressed as a function of the isotropic luminosity (\tilde{L}_{iso}) by combining the ‘‘Yonetoku relation’’ [56] and the Amati one [57] for the long-duration GRBs [32]:

$$\log \left(\frac{\tilde{E}_{\text{iso}}}{10^{52} \text{ erg}} \right) = 1.07 \log \left(\frac{\tilde{L}_{\text{iso}}}{10^{52} \text{ erg/s}} \right) + (0.66 \pm 0.54). \quad (2.7)$$

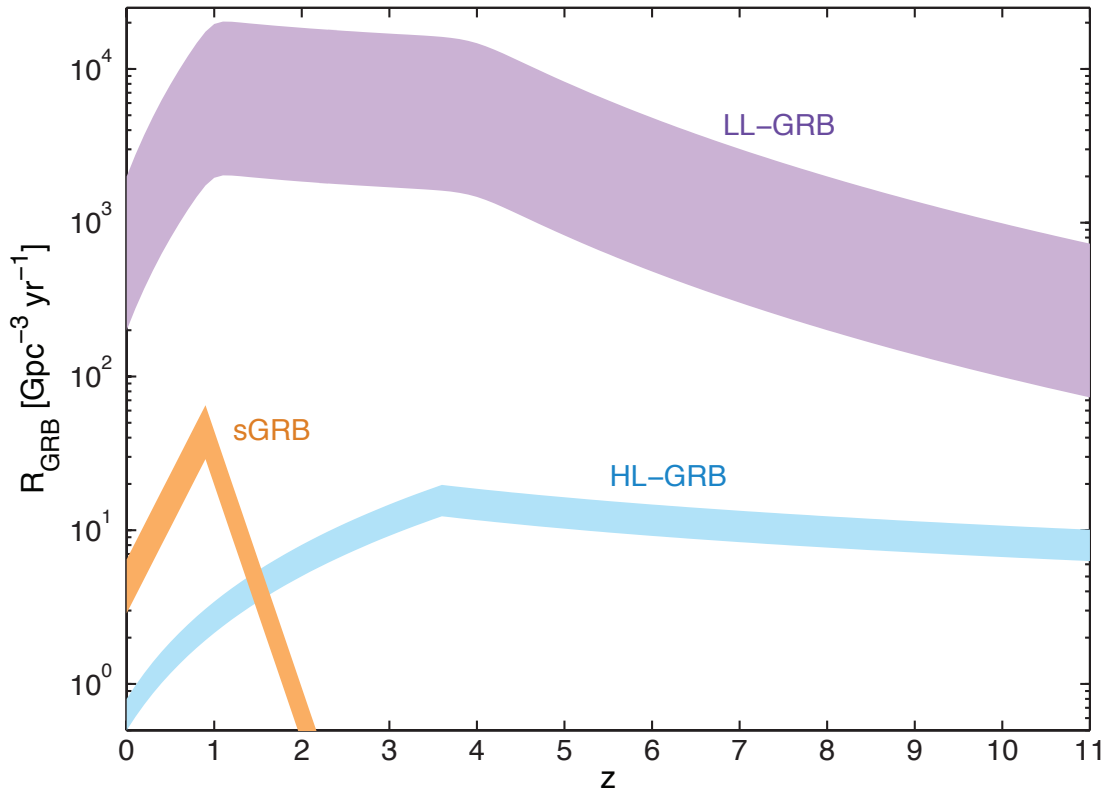


Figure 1. Redshift distribution of the HL-GRBs (light blue), LL-GRBs (violet), and sGRBs (orange). Each family is normalised to its local rate ρ_0 . The LL-GRB local rate is higher than the HL-GRB and the sGRB ones, and the sGRB rate quickly decreases for $z \geq 1$.

In the following, we will assume that the Amati and Yonetoku relations hold for both the LL- and HL-GRBs, postulating that the two populations share the same emission mechanism (see e.g. [48, 58] for a discussion on the topic).

The photon break energy in the jet frame is related to the same quantity in the GRB frame through $E'_{\gamma,b} = \tilde{E}_{\gamma,b}/\Gamma$. The normalisation of the photon spectrum, f_γ , is set by assuming that $f_\gamma = \tilde{E}_{\text{iso}} / \int_0^\infty d\tilde{E}_\gamma \tilde{E}_\gamma (dN_\gamma/d\tilde{E}_\gamma)$.

2.2 Short-duration gamma-ray bursts

Short-duration GRBs (sGRB) exhibit typical luminosities similar to those of the HL-GRBs, and are believed to originate from neutron-star–neutron-star or neutron-star–black-hole mergers [7]. Therefore, we should expect a delay between the star-formation rate and the merger rate due to the spiral-in time [59, 60]. In order to model the sGRB redshift distribution and their luminosity function, we follow [61] which selects a sample of non-collapsar GRBs from the BATSE, *Swift*, and *Fermi* data.

The sGRB rate is described by the convolution of the ordinary star-formation rate with a function $f(\Delta t)$ that takes into account the time-delay Δt of the spiral-in time of the binaries [59, 60]. According to [61], the time-delay function that is in better agreement with the data is a log-normal distribution that allows to express the sGRB formation with the

following effective rate:

$$R_{\text{sGRB}} = 10 \rho_0 \begin{cases} \exp[(z - 0.9)/0.39] & \text{for } z \leq z_\star \\ \exp[-(z - 0.9)/0.26] & \text{for } z > z_\star \end{cases}, \quad (2.8)$$

with $z_\star = 0.9$. The sGRB rate as a function of the redshift is plotted in Fig. 1 (orange band), note as it peaks at about z_\star and then it decreases quickly. The sGRB rate is locally higher than the HL-GRB one.

The LF is fitted with a broken power law [61]:

$$\Phi_{\text{sGRB}} \propto \begin{cases} \left(\frac{\tilde{L}_{\text{iso}}}{L_\star}\right)^\alpha & \text{for } \tilde{L}_{\text{iso}} \leq L_\star \\ \left(\frac{\tilde{L}_{\text{iso}}}{L_\star}\right)^\beta & \text{for } \tilde{L}_{\text{iso}} > L_\star \end{cases}, \quad (2.9)$$

with the best fit parameters provided in Table 1.

Similarly to the long-duration GRBs, sGRBs have a gamma-ray spectrum fitted with the Band spectrum (Eq. 3.19). However, we know from observations that the low-energy component (i.e., for $E_\gamma < E_{\gamma,b}$) is harder for sGRBs than for the long-duration GRBs (see the values for α_γ in Table 1) and the peak energy is slightly higher [61–63].

We assume that relations similar to the Amati and Yonetoku ones hold between $\tilde{E}_{\gamma,b}$, \tilde{E}_{iso} , and \tilde{L}_{iso} for the sGRBs. To this purpose, we extrapolate them by fitting the data in Fig. 7 of [63] and define the analogous of Eqs. (2.6) and (2.7):

$$\log\left(\frac{\tilde{E}_{\gamma,b}}{0.1 \text{ MeV}}\right) = 0.56 \log\left(\frac{\tilde{E}_{\text{iso}}}{10^{52} \text{ erg}}\right) + 3.23, \quad (2.10)$$

$$\log\left(\frac{\tilde{E}_{\text{iso}}}{10^{52} \text{ erg}}\right) = 1.06 \log\left(\frac{\tilde{L}_{\text{iso}}}{10^{52} \text{ erg/s}}\right) - 1.57. \quad (2.11)$$

We suppose that this class of GRBs has shorter variability timescale (t_v) than long-duration GRBs [64], as reported in Table 1.

3 Prompt neutrino emission from gamma-ray burst fireballs

In this Section, we discuss the neutrino production in GRBs through $p\gamma$ interactions and derive the corresponding neutrino energy distributions. The main reactions that we study are:

$$\begin{aligned} p + \gamma &\rightarrow \Delta \rightarrow n + \pi^+, p + \pi^0 \\ p + \gamma &\rightarrow K^+ + \Lambda/\Sigma \end{aligned} \quad (3.1)$$

Pions, kaons and neutrons in turn decay into neutrinos:

$$\begin{aligned} \pi^+ &\rightarrow \mu^+ \nu_\mu, \\ \mu^+ &\rightarrow \bar{\nu}_\mu + \nu_e + e^+, \\ \pi^- &\rightarrow \mu^- \bar{\nu}_\mu, \\ \mu^- &\rightarrow \nu_\mu + \bar{\nu}_e + e^-, \\ K^+ &\rightarrow \mu^+ + \nu_\mu, \\ n &\rightarrow p + e^- + \bar{\nu}_e. \end{aligned} \quad (3.2)$$

In the following, we will assume that the neutrino contribution from the n decay is negligible (see Fig. 2 of [65]) and we will reconstruct the neutrino energy spectrum from the pion and kaon decays.

3.1 Neutrino production from pion decay

The comoving proton energy threshold to produce a Δ resonance is $E'_p \geq [(m_\Delta c^2)^2 - (m_p c^2)^2]/(4E'_\gamma)$, where m_Δ (m_p) is the Δ (p) mass. The corresponding neutrino energy in the observer frame is [66]: $E_\nu = 0.05 [\Gamma/(1+z)]^2 (m_\Delta^2 - m_p^2)/(2E_\gamma)$, with Γ the bulk Lorentz factor of the jet that we assume constant for sake of simplicity; the numerical factor comes from the fact that the average energy fraction transferred from the initial proton to the pion is 20% times 1/4 which comes from the assumption that the 4 leptons in the π decay channel equally share the energy of the pion (i.e., $E_\nu = 0.05 E_p$).

The resultant neutrino spectrum will exhibit a spectral break at:

$$E_{\nu,b,\pi} = a_\pi \left(\frac{\Gamma}{1+z} \right)^2 \frac{(m_\Delta c^2)^2 - (m_p c^2)^2}{2E_{\gamma,b}} = 1.6 \times 10^6 E_{\gamma,b,\text{MeV}}^{-1} \left(\frac{\Gamma_{2.5}}{1+z} \right)^2 \text{ GeV}, \quad (3.3)$$

where, in the first equality, the correction factor of 2 with respect to E'_p takes into account the fact that the pion production efficiency peaks at higher center of mass energies [65]. The pre-factor a_π for neutrinos produced by pion decay is $a_\pi = 0.05 = 0.2 \times 1/4$ (since 20% is the fraction of the proton energy that goes into pion and 1/4 is the fraction of the π energy carried by neutrinos). In order to favor a comparison with the existing literature, in the second equality, we express it in terms of typical values for the GRB parameters: $\Gamma_{2.5} = \Gamma/10^{2.5}$ and $E_{\gamma,b,\text{MeV}} = E_{\gamma,b}/\text{MeV}$.

Above $E_{\nu,b,\pi}$, the neutrino spectrum is the same as the proton spectrum, because the protons can interact with photons with energies $E_{\gamma,b}$ or smaller, where the number of photons is almost constant, i.e., $E_\gamma dN_\gamma/dE_\gamma \propto E_\gamma^{1-\alpha_\gamma} = E_\gamma^0$. Below $E_{\nu,b,\pi}$, on the other hand, the number of photons with energy E_γ that a proton with energy E_p/a_π can interact with is suppressed by a factor of $(E_\gamma/E_{\gamma,b})^{1-\beta_\gamma} = (E_{\nu,b,\pi}/E_p)^{1-\beta_\gamma}$, and the resulting neutrino spectrum is harder by a factor of $E_p^{\beta_\gamma-1}$ with respect to the proton spectrum (that we assume to scale as $\sim E_p^{-2}$).

If pions produced by the $p\gamma$ interactions decay faster than they cool, the correspondent neutrino spectrum is not affected. Otherwise, other neutrino break energies are determined by the radiative cooling (rc; synchrotron radiation and inverse Compton scattering), adiabatic cooling (ac), and hadronic cooling (hc) processes, being the total cooling timescale defined as $t'_c{}^{-1} = t'_{\text{hc}}{}^{-1} + t'_{\text{rc}}{}^{-1} + t'_{\text{ac}}{}^{-1}$. The neutrino spectrum is modified by an additional factor of $[1 - \exp(-t'_c m_\pi/E'_\pi \tau_\pi)]$, where τ_π is the pion lifetime and m_π is the pion mass. If the cooling time scale is much shorter than the decay lifetime in the jet frame (i.e., $t'_c \ll E'_\pi \tau_\pi/m_\pi$), the additional factor can be approximated as $t'_c m_\pi/E'_\pi \tau_\pi$. Below, we shall discuss the three relevant cooling processes.

The hadronic cooling timescale for pions in the jet frame is:

$$t'_{\pi,\text{hc}} = \frac{E'_\pi}{c\sigma_h n'_p \Delta E'_\pi} = \frac{20\pi c^4 \Gamma^6 m_p t_v^2 \epsilon_e}{0.3\sigma_h \tilde{L}_{\text{iso}}(1+z)^2}, \quad (3.4)$$

where c is the speed of light, $n'_p = E_j(1+z)/(\Gamma m_p c^2 V')$ the jet comoving proton density, $\sigma_h = 5 \times 10^{-26} \text{ cm}^2$ [67] the cross section for meson-proton collisions, and $\Delta E'_\pi$ the energy lost by the incident meson in each collision, which is $\Delta E'_\pi = 0.8E'_\pi$ [68]. For a jet with kinetic

energy E_j , opening angle θ_j and variability timescale t_v , the volume of an infinitesimal jet shell is $V' = 2\pi\theta_j^2\tilde{r}_j^2ct_j\Gamma/(1+z)$ with $\tilde{r}_j = 2\Gamma^2ct_v/(1+z)$ the internal shock radius. We then converted the jet energy E_j divided by the duration t_j (the jet luminosity $L_j = E_j/t_j$) into the isotropic peak luminosity via $L_j/(2\pi\theta_j^2) = 0.3\tilde{L}_{\text{iso}}/[4\pi(1+z)^2\epsilon_e]$, where 0.3 comes from the fact that typically 0.3 times the peak luminosity is the luminosity averaged over the duration of the burst [32, 69], and ϵ_e is the energy fraction carried by the electrons. When the hadronic cooling is the dominant cooling process (i.e., $t'_c \simeq t'_{\pi,\text{hc}}$), a steepening of the neutrino energy spectrum occurs at an energy satisfying $t'_{\text{hc}} = \tau_\pi E'_\pi/(m_\pi c^2)$ with τ_π (m_π) the pion lifetime (mass), i.e.,

$$E_{\nu,\pi,\text{hc}} = \frac{b_\pi\Gamma}{(1+z)^3} \frac{20\pi m_\pi m_p c^6 \Gamma^6 t_v^2 \epsilon_e}{0.3\tau_\pi \sigma_h \tilde{L}_{\text{iso}}} = 1.75 \times 10^{13} \frac{\Gamma_{2.5}^7 t_{v,-2}^2 \epsilon_e}{(1+z)^3 \tilde{L}_{\text{iso},52}} \text{ GeV} , \quad (3.5)$$

where $b_\pi = 1/4$, $E'_\nu = E'_\pi/4$, $t_{v,-2} = t_v/(10^{-2} \text{ s})$, and $\tilde{L}_{\text{iso},52} = \tilde{L}_{\text{iso}}/(10^{52} \text{ erg s}^{-1})$. Since $t'_{\pi,\text{hc}}$ is independent of energy, the neutrino spectrum suppression factor due to the hadronic cooling is $t'_{\text{hc}}m_\pi/(E'_\pi\tau_\pi) \propto 1/E'_\nu$.

The adiabatic cooling time in the jet comoving frame is given by

$$t'_{\pi,\text{ac}} = \frac{\tilde{r}_j}{\Gamma c} , \quad (3.6)$$

which is energy independent. By solving $t'_{\pi,\text{ac}} = \tau_\pi E'_\pi/(m_\pi c^2)$, we find that the neutrino spectrum breaks at

$$E_{\nu,\pi,\text{ac}} = \frac{b_\pi\Gamma^2}{(1+z)^2} \frac{2m_\pi c^2 t_v}{\tau_\pi} = 2.7 \times 10^9 \frac{\Gamma_{2.5}^2 t_{v,-2}}{(1+z)^2} \text{ GeV} , \quad (3.7)$$

and it steepens with respect to the parent spectrum by $1/E'_\nu$.

The radiative cooling time is given by

$$t'_{\pi,\text{rc}} = \frac{3m_\pi^4 c^3}{4\sigma_T m_e^2 E'_\pi (U'_B + U'_\gamma)} = \frac{3\pi c^6 m_\pi^4 \Gamma^6 t_v^2}{0.3\sigma_T m_e^2 E'_\pi \tilde{L}_{\text{iso}} (1+z)^2 (1 + \epsilon_B/\epsilon_e)} , \quad (3.8)$$

where $U'_B = B'^2/(8\pi) = 4\epsilon_B E'_j/V'$ defined in terms of the fraction of the internal energy carried by the magnetic field (ϵ_B), $U'_\gamma = E'_\gamma n'_\gamma = 4E'_j \epsilon_e/V'$,¹ m_e the electron mass and σ_T the Thomson cross section. Note that $t'_{\pi,\text{rc}} \propto 1/E'_\pi$. When $t'_c \simeq t'_{\pi,\text{rc}}$ and the other cooling processes do not play a role at any relevant energies, a break energy in the neutrino spectrum is expected for $t'_{\pi,\text{rc}} = \tau_\pi E'_\pi/(m_\pi c^2)$:

$$E_{\nu,\pi,\text{rc}} = \frac{b_\pi\Gamma}{(1+z)^2} \left[\frac{3\pi c^8 m_\pi^5 \Gamma^6 t_v^2}{0.3\tau_\pi \sigma_T m_e^2 \tilde{L}_{\text{iso}} (1 + \epsilon_B/\epsilon_e)} \right]^{1/2} = 1.8 \times 10^8 \frac{\Gamma_{2.5}^4 t_{v,-2}}{(1+z)^2 [\tilde{L}_{\text{iso},52} (1 + \epsilon_B/\epsilon_e)]^{1/2}} \text{ GeV} , \quad (3.9)$$

and the radiative cooling is responsible for a steepening of the correspondent neutrino spectrum by a factor $\propto 1/E'_\nu{}^2$.

¹The numerical factor 4 in the definition of U'_B and U'_γ comes from the fact that, assuming that the upstream material is cold while the shock wave is propagating, the relativistic strong shock transition relations predict a post-shock energy density $U_2 = 4\Gamma_{21}^2 n_1 \epsilon$, being $\Gamma_{21} \simeq 1$ the relative Lorentz factor for the internal shock model and n_1 the density before the shock front, and ϵ the energy carried by the particle [2].

If the hadronic cooling occurs at energies lower than the ones for which the radiative cooling dominates, the transition between the two cooling mechanisms happens at the neutrino break energy corresponding to $t'_{\pi,\text{hc}} = t'_{\pi,\text{rc}}$ instead of $t'_{\pi,\text{rc}} = \tau_\pi E'_\pi / (m_\pi c^2)$; it is:

$$E_{\nu,\pi,\text{rc},2} = \frac{b_\pi \Gamma}{(1+z)} \frac{3c^2 m_\pi^4 \sigma_h}{20m_p m_e^2 \sigma_T (\epsilon_e + \epsilon_B)} = 1.4 \times 10^3 \frac{\Gamma_{2.5}}{(1+z)(\epsilon_e + \epsilon_B)} \text{GeV} . \quad (3.10)$$

Similarly, if the adiabatic cooling occurs before the radiative cooling, the break energy in the neutrino spectrum due to the radiative cooling is determined by $t'_{\pi,\text{ac}} = t'_{\pi,\text{rc}}$:

$$E_{\nu,\pi,\text{rc},3} = \frac{b_\pi \Gamma^6}{(1+z)^2} \frac{5\pi c^6 m_\pi^4 t_v}{(1+\epsilon_B/\epsilon_e) \tilde{L}_{\text{iso}} m_e^2 \sigma_T} = 1.2 \times 10^7 \frac{\Gamma_{2.5}^6 t_{v,-2}}{(1+z)^2 (1+\epsilon_B/\epsilon_e) \tilde{L}_{\text{iso},52}} \text{GeV} . \quad (3.11)$$

In both cases the correspondent neutrino spectrum will be subject to a further $1/E'_\nu$ steepening with respect to the one affected by hadronic or adiabatic cooling.

Muons produced by the pion decay (from now on indicated as μ_π) will in turn originate a neutrino energy spectrum, with a first break energy defined similarly to the one in Eq. (3.3), but with the pre-factor $a_{\mu_\pi} = 0.05 = 0.2 \times 3/4 \times 1/3$ (where $3/4$ is the energy fraction transferred from pions to muons, and $1/3$ is due to three-body decay of the muon). In terms of typical GRB parameters, it can be written as

$$E_{\nu,b,\mu_\pi} = 1.6 \times 10^6 E_{\gamma,b,\text{MeV}}^{-1} \left(\frac{\Gamma_{2.5}}{1+z} \right)^2 \text{GeV} , \quad (3.12)$$

Other energy breaks in the neutrino spectrum are determined by the radiative cooling processes ($t'_{\mu,\text{rc}} \simeq \tau_\mu E'_\mu / (m_\mu c^2)$):

$$E_{\nu,\mu,\text{rc}} = \frac{b_\mu \Gamma}{(1+z)^2} \left[\frac{3\pi c^8 m_\mu^5 \Gamma^6 t_v^2}{0.3\tau_\mu \sigma_T m_e^2 \tilde{L}_{\text{iso}} (1+\epsilon_B/\epsilon_e)} \right]^{1/2} = 1.3 \times 10^7 \frac{\Gamma_{2.5}^4 t_{v,-2}}{(1+z)^2 [\tilde{L}_{\text{iso},52} (1+\epsilon_B/\epsilon_e)]^{1/2}} \text{GeV} , \quad (3.13)$$

with $b_\mu = 1/3$ since $E'_\nu = E'_\mu/3$. Note as the break energy $E_{\nu,\mu,\text{rc}}$ is usually one order of magnitude smaller than the pion one (Eq. 3.9), due to difference in the masses and lifetimes of the two particles. Similarly to pions, muons are also subject to adiabatic cooling. In this case, the correspondent break energies in the neutrino spectrum are

$$E_{\nu,\mu,\text{ac}} = \frac{b_\mu \Gamma^2}{(1+z)^2} \frac{2m_\mu c^2 t_v}{\tau_\mu} = 3.2 \times 10^7 \frac{\Gamma_{2.5}^2 t_{v,-2}}{(1+z)^2} \text{GeV} , \quad (3.14)$$

$$E_{\nu,\mu,\text{rc},3} = \frac{b_\mu \Gamma^6}{(1+z)^2} \frac{5\pi c^6 m_\mu^4 t_v}{(1+\epsilon_B/\epsilon_e) \tilde{L}_{\text{iso}} m_e^2 \sigma_T} = 5.4 \times 10^6 \frac{\Gamma_{2.5}^6 t_{v,-2}}{(1+z)^2 (1+\epsilon_B/\epsilon_e) \tilde{L}_{\text{iso},52}} \text{GeV} \quad (3.15)$$

Assuming that $E'_\pi = 4E_\nu(1+z)/\Gamma$ and $E'_\mu = 3E_\nu(1+z)/\Gamma$, the relations among the comoving muon and pion lifetimes and the cooling times as from Eqs. (3.4), (3.6), (3.8) and the correspondent ones for muons are shown in the top panels of Figs. 2, 3 and 4 for typical HL-, LL-GRB and sGRBs at $z = 1$. We took $\tilde{L}_{\text{iso}} = 10^{52}$ erg/s for the HL-GRBs, $\tilde{L}_{\text{iso}} = 10^{48}$ erg/s for the LL-GRB, and $\tilde{L}_{\text{iso}} = 10^{51}$ erg/s for the sGRBs. For each family, we supposed Γ and t_v as in Table 1 and defined $\epsilon_e = \epsilon_B = 10^{-2}$ for HL-GRBs and sGRBs, while we adopted $\epsilon_e = \epsilon_B = 10^{-3}$ for LL-GRBs (see Sec. 3.3).

For the GRB parameters assumed in Figs. 2, 3 and 4, the hadronic cooling is negligible for HL-GRBs and sGRBs. On the other hand, the radiative cooling and the adiabatic one

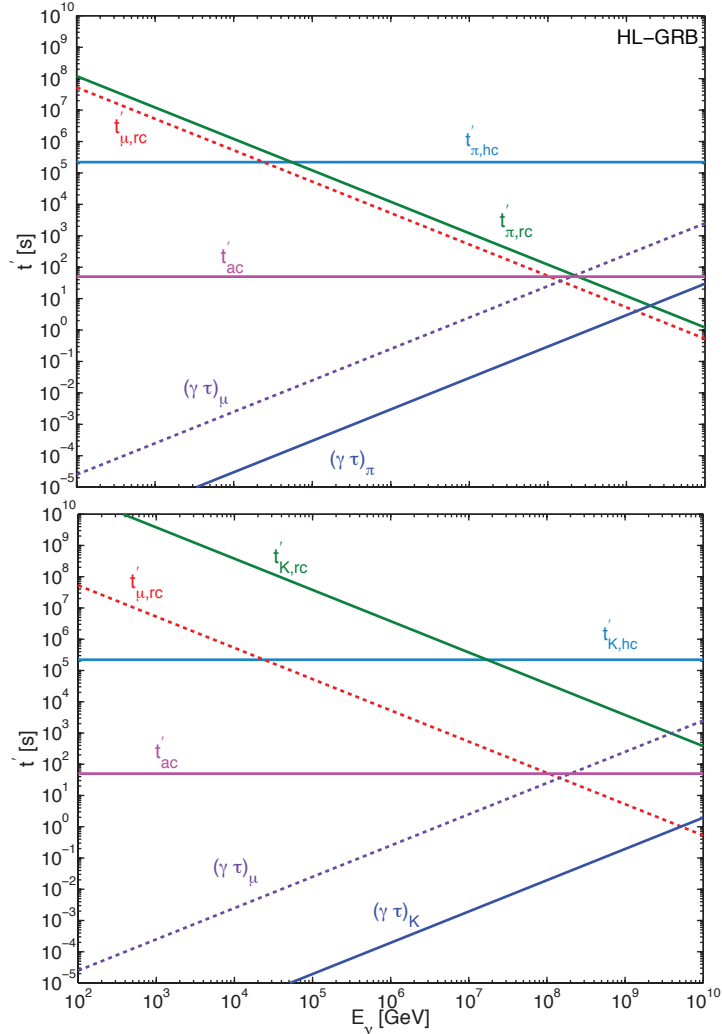


Figure 2. Top panel: Muon and pion lifetimes and cooling times in the jet comoving frame as a function of the neutrino energy E_ν for a typical HL-GRB with $\tilde{L}_{\text{iso}} = 10^{52}$ erg/s and $z = 1$. Bottom panel: Muon and kaon lifetimes and cooling times for the same HL-GRB. For the assumed HL-GRB parameters, the radiative cooling is always important, while the hadronic cooling is negligible and the adiabatic cooling is relevant for muons.

are always relevant for all three families for both pions and muons. As we will discuss in the following, note as such hierarchy among the cooling processes is a function of \tilde{L}_{iso} and z for other fixed GRB parameters. Therefore it will change within the luminosity and redshift range that we will consider for the computation of the diffuse neutrino emission.

3.2 Neutrino production from kaon decay

Yet another contribution to the total neutrino spectrum from GRBs originates from kaon decays. The resultant neutrino spectrum will have a first break energy coming from the

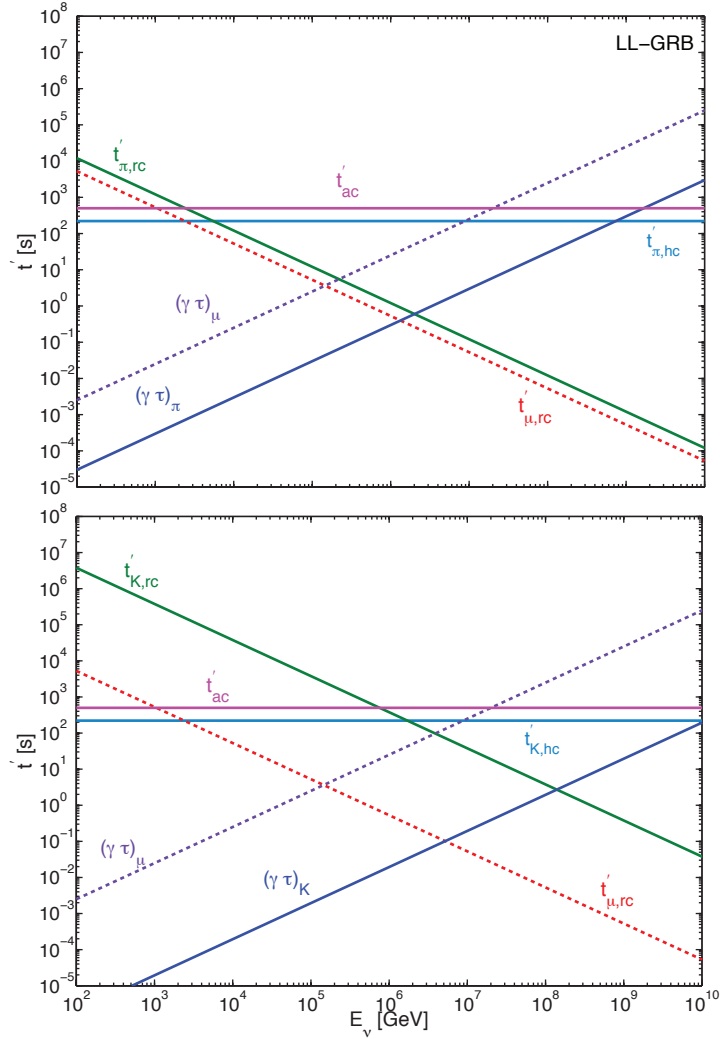


Figure 3. The same as Fig. 2, but for a typical LL-GRB with $\tilde{L}_{\text{iso}} = 10^{48}$ erg/s and $z = 1$. For the assumed LL-GRB parameters, the adiabatic and the hadronic cooling are negligible for kaons.

proton threshold energy for kaon production, similarly to Eq. (3.3):

$$E_{\nu,b,i} = c_i \left(\frac{\Gamma}{1+z} \right)^2 \frac{(m_K c^2 + m_\Lambda c^2)^2 - (m_p c^2)^2}{2E_{\gamma,b}}, \quad (3.16)$$

where, for neutrinos directly produced from kaon decay without going through muons, $c_K = 0.1$ (since 20% is the fraction of the proton energy that goes into K and 1/2 is the fraction of K energy carried by neutrinos). In the case of muons originating from kaon decay, from now on indicated as μ_K to distinguish them from the ones from muon decay (μ_π), $c_{\mu_K} = 0.033 = 0.2 \times 1/2 \times 1/3$. In terms of typical parameters, the first break energies for K and

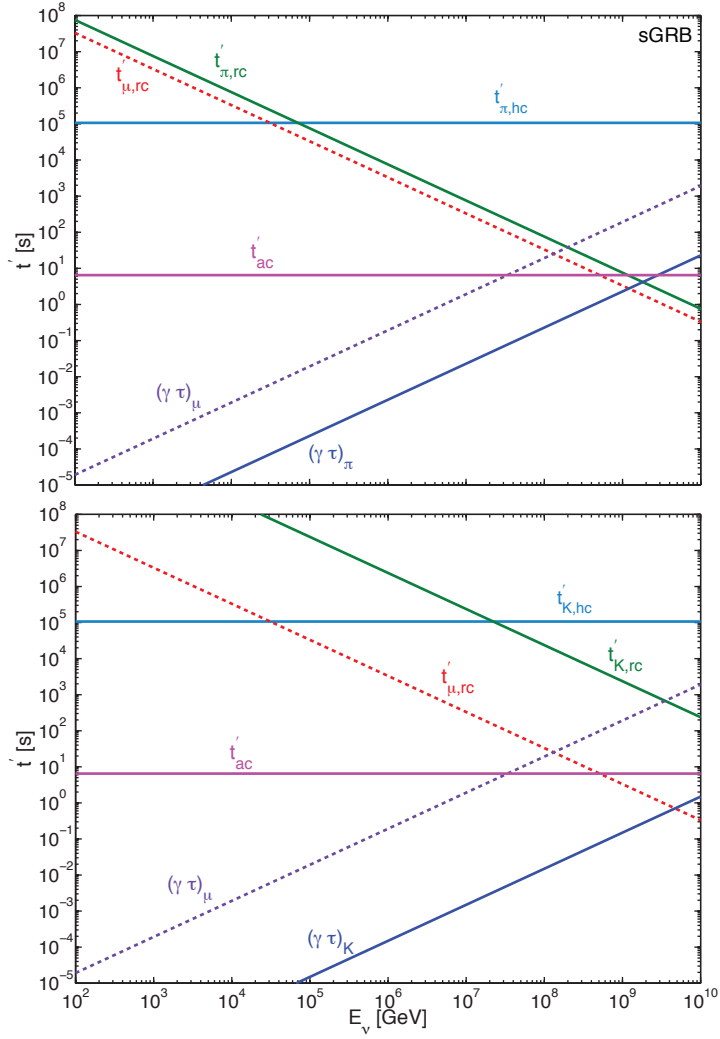


Figure 4. The same as Fig. 2, but for a typical sGRB with $\tilde{L}_{\text{iso}} = 10^{51}$ erg/s and $z = 1$. For the assumed sGRB parameters, the hadronic cooling is negligible.

μ_K become:

$$E_{\nu,b,K} = 8.5 \times 10^6 E_{\gamma,b,\text{MeV}}^{-1} \left(\frac{\Gamma_{2.5}}{1+z} \right)^2 \text{ GeV} , \quad (3.17)$$

$$E_{\nu,b,\mu_K} = 2.6 \times 10^6 E_{\gamma,b,\text{MeV}}^{-1} \left(\frac{\Gamma_{2.5}}{1+z} \right)^2 \text{ GeV} . \quad (3.18)$$

The resultant neutrino spectrum from kaon decay is affected, similarly to what was discussed for pions, from hadronic, adiabatic, and radiative cooling processes. Therefore, we should expect breaks in the neutrino spectrum similar to the ones described in Eqs. (3.5), (3.7), (3.9), (3.10), and (3.11) according to the cases, but with the substitution $m_\pi(\tau_\pi) \rightarrow m_K(\tau_K)$. For example, $E_{\nu,K,\text{rc}}$ will be $d_K \Gamma / (1+z)^2 [4\pi c^8 m_\pi^5 \Gamma^6 t_v^2 / (0.3\tau_\pi \sigma_T m_e^2 \tilde{L}_{\text{iso}} (1+\epsilon_B/\epsilon_e))]^{1/2}$, with $d_K = 1/2$ since $E'_\nu = E'_K/2$. Similarly, the equations in terms of typical parameters

can be extrapolated from the ones from pions rescaling $m_\pi(\tau_\pi)$ to $m_K(\tau_K)$ and taking into account the different multiplicity factors.

Muons are also produced from kaon decay. The resultant neutrino energy spectrum will be determined as the one described for muons from pion decay (see Eqs. 3.13, 3.14 and 3.15).

The bottom panels of Figs. 2, 3 and 4 show the relations among the muon and kaon lifetimes and the cooling times, similarly to the top panels for pions and muons from pion decays, assuming that $E'_K = 2E_\nu(1+z)/\Gamma$ and $E'_\mu = 3E_\nu(1+z)/\Gamma$. The hadronic cooling is negligible, while the adiabatic cooling is relevant for muons for the model parameters plotted in these figures. Note that the break energies in the neutrino spectrum due to the kaon radiative cooling occur at higher energies than the ones due to pion radiative cooling given the differences in the rest-mass and lifetimes of the two parent particles [70, 71]. We neglect here the contribution to the neutrino flux coming from K^0 , see Ref. [38] for a dedicated discussion.

3.3 Neutrino energy spectra

As discussed in the previous section, the neutrino energy spectrum for one flavor ($\nu + \bar{\nu}$) resulting from π , K , and μ decays will be a broken power law derived from the parent proton spectrum (that we assume is proportional to E_p^{-2}) with further breaks defined according to the hierarchy of the cooling processes. For example, when the pion hadronic cooling is negligible, the adiabatic cooling is relevant for muons only, and $E'_{\nu,b,\mu} < E'_{\nu,\mu,ac} < E'_{\nu,\mu,rc,3} < E'_{\nu,\pi,rc}$, the resultant neutrino energy spectrum produced from muons from pion decay will be:

$$\left(\frac{dN_\nu}{dE'_\nu}\right)_{inj,\mu\pi} \propto \begin{cases} \left(\frac{E'_\nu}{E'_{\nu,b,\mu}}\right)^{\beta_\gamma-3} & \text{for } E'_\nu < E'_{\nu,b,\mu} \\ \left(\frac{E'_\nu}{E'_{\nu,b,\mu}}\right)^{\alpha_\gamma-3} & \text{for } E'_{\nu,b,\mu} \leq E'_\nu < E'_{\nu,\mu,ac} \\ \left(\frac{E'_{\nu,\mu,ac}}{E'_{\nu,b,\mu}}\right)^{\alpha_\gamma-3} \left(\frac{E'_\nu}{E'_{\nu,\mu,ac}}\right)^{\alpha_\gamma-4} & \text{for } E'_{\nu,\mu,ac} \leq E'_\nu < E'_{\nu,\mu,rc,3} \\ \left(\frac{E'_{\nu,\mu,ac}}{E'_{\nu,b,\mu}}\right)^{\alpha_\gamma-3} \left(\frac{E'_{\nu,\mu,rc,3}}{E'_{\nu,\mu,ac}}\right)^{\alpha_\gamma-4} \left(\frac{E'_\nu}{E'_{\nu,\mu,rc,3}}\right)^{\alpha_\gamma-5} & \text{for } E'_{\nu,\mu,rc,3} \leq E'_\nu < E'_{\nu,\pi,rc} \\ \left(\frac{E'_{\nu,\mu,ac}}{E'_{\nu,b,\mu}}\right)^{\alpha_\gamma-3} \left(\frac{E'_{\nu,\mu,rc,3}}{E'_{\nu,\mu,ac}}\right)^{\alpha_\gamma-4} \left(\frac{E'_{\nu,\pi,rc}}{E'_{\nu,\mu,rc,3}}\right)^{\alpha_\gamma-5} \left(\frac{E'_\nu}{E'_{\nu,\pi,rc}}\right)^{\alpha_\gamma-7} & \text{for } E'_\nu \geq E'_{\nu,\pi,rc} \end{cases} \quad (3.19)$$

For each decay channel i , the neutrino energy spectrum is normalized in terms of the total photon fluence by generalizing the expression proposed in Refs. [10, 72]:

$$\int_0^\infty dE_\nu E_\nu \left(\frac{dN_\nu}{dE_\nu}\right)_{inj,i} = N_i \frac{h_{p,i}}{h_{\gamma p}} [1 - (1 - \langle\chi_p\rangle)^{\tau_{p\gamma}}] \int_0^\infty dE_\gamma E_\gamma \left(\frac{dN_\gamma}{dE_\gamma}\right)_{inj}. \quad (3.20)$$

In our numerical computations within the *canonical* model, we assume the gamma-ray-proton luminosity ratio $h_{\gamma p} = L_{iso}/L_p = 10^{-2}$ for HL-GRBs and sGRBs as suggested by joint analysis of high-energy neutrino and ultrahigh-energy cosmic ray (UHECR) data [28, 30] and under the assumption that sGRBs behave similarly to HL-GRBs; while we adopt $h_{\gamma p} = 10^{-3}$ for the LL-GRB family assuming that the γ production is suppressed in these GRBs with respect to the other two GRB families for the same L_p^2 . We will discuss in detail the

²Note as, assuming $L_j = L_p + L_e + L_B$ and $\epsilon_e \simeq \epsilon_B$, one has that $h_{\gamma p} \simeq \epsilon_e/(1 - \epsilon_e - \epsilon_B) \sim \epsilon_e$. This justifies the choice of the numerical values of ϵ_e and ϵ_B introduced in Sec. 3 and adopted through the whole paper.

dependence of the diffuse background from this parameter in Sec. 4.2. For the case of neutrinos produced from the pion decay, $N_\pi = 0.97/8$ (the coefficient $1/8 = 1/4 \times 1/2$ since each neutrino takes about $1/4$ of the pion energy and $1/2$ of the produced pions are charged pions, while 97% is the probability that pions are produced from one $p\gamma$ interaction [73, 74]) and $h_{p,\pi} \simeq \ln(E_{\nu,\pi,\text{second}}/E_{\nu,\pi,\text{first}})/\ln(E_{p,\text{max}}/E_{p,\text{min}})$ with $E_{\nu,\pi,\text{first}}$ the minimum neutrino break energy and $E_{\nu,\pi,\text{second}}$ the second neutrino break energy, both defined according to the hierarchy of the break energies determined by the cooling processes and $E_{\nu,b,\mu}$. Note that, for each GRB family and fixed parameters, such energy hierarchy varies as a function of \tilde{L}_{iso} and z . The minimum proton energy is $E_{p,\text{min}} = \Gamma m_p c^2 / (1+z)$ while the maximum proton energy is $E_{p,\text{max}}$ and it is defined as the energy when the acceleration time $t'_{p,\text{acc}} = E'_p / (B'ec)$ equals to $t'_{p,c} = \min(t'_{p,\text{sync}}, t'_{p,\text{dyn}})$, being $t'_{p,\text{sync}} = (3m_p^4 c^3 8\pi) / (4\sigma_T m_e^2 E'_p B'^2)$ the synchrotron cooling time and $t'_{p,\text{dyn}} = r'_j / c$ the dynamical time scale. For μ produced from π decay, $N_{\mu\pi} = 0.97/3 \times 3/8 = N_\pi$ and $h_{p,\mu\pi} \simeq \ln(E_{\nu,\mu,\text{second}}/E_{\nu,\mu,\text{first}})/\ln(E_{p,\text{max}}/E_{p,\text{min}})$ defined analogously to $h_{p,\mu}$.

In the case of neutrino production from kaon decay, $N_K = 0.03 \times 0.63/2$ where the numerical coefficient $1/2$ comes from the fact that each neutrino takes about $1/2$ of the kaon's energy, 0.63 is the probability that K decays in neutrinos, and 3% the probability that kaons are produced from one $p\gamma$ interaction [73, 74]. The term $h_{p,K} \simeq \ln(E_{\nu,K,\text{second}}/E_{\nu,K,\text{first}})/\ln(E_{p,\text{max}}/E_{p,\text{min}})$ is defined similarly as $h_{p,\pi}$. For muons generated from kaon decay, we have $N_{\mu K} = 0.03 \times 0.63/6$.

The second term in Eq. (3.20), $f = [1 - (1 - \langle\chi_p\rangle)^{\tau_{p\gamma}}]$, represents the fraction of the proton energy that goes to pion production with $\langle\chi_p\rangle \simeq 0.2$ the average fraction of energy transferred from protons to pions or kaons per $p\gamma$ interaction [10, 15]. The $p\gamma$ optical depth, $\tau_{p\gamma}$, is defined following [8, 9, 15]:

$$\tau_{p\gamma} = \frac{\tilde{r}_j}{\Gamma \ell_{p\gamma}} = 0.6 \frac{\tilde{L}_{\text{iso}}}{10^{52} \text{ erg/s}} \left(\frac{\Gamma}{10^{2.5}} \right)^{-2} \left(\frac{\tilde{r}_j}{10^{14} \text{ cm}} \right)^{-1}, \quad (3.21)$$

with $\ell_{p\gamma}$ the mean free path for $p\gamma$ interactions. Note that with respect to the numerical fireball model revised in [10], we do include their correction term c_s (originally introduced in [72]), but do not implement the factor c_{f_π} due to the pion efficiency (see [10] for details). The latter is responsible for a further reduction of the expected neutrino flux with respect to the one obtained from our Eq. (3.20), as shown in the left panel of Fig. 1 of [10]. We also neglect multi-pion processes that should be instead responsible for an enhancement of the neutrino flux (see right panel of Fig. 1 of Ref. [10], comparison between their RFC and NFC models). Therefore our analytical model is still an approximation with respect to the full numerical treatment, but it gives us results in good agreement with the revised fireball model of [10] for the same choice of the initial parameters.

In order to consistently normalize the neutrino spectrum as in Eq. (3.20), we need to select the GRB parameters in such a way to have optically thin media [8]. Therefore, we consider a test photon with energy $E_{\gamma,t} = 100$ MeV and define the $\gamma\gamma$ optical depth

$$\tau_{\gamma\gamma} = \frac{\tilde{r}_j}{\Gamma \ell_{\gamma\gamma}} = \frac{(1+z)^2 \sigma_T 0.3 \tilde{L}_{\text{iso}} E_{\gamma,t}}{128\pi \Gamma^6 c^2 t_v (m_e c^2)^2}, \quad (3.22)$$

with the mean free path for pair production $\ell_{\gamma\gamma}^{-1} \simeq (\sigma_T U'_\gamma E'_{\gamma,t}) / [16(m_e c^2)^2]$ and $\tilde{L}_{\text{ave}} = 0.3 \tilde{L}_{\text{iso}} = 4\pi \tilde{r}_j^2 \Gamma^2 c U'_\gamma$ [8, 9]. In our *canonical* GRB model, we fix t_v to the average value preferred by observations [23, 64, 75] and define Γ as the minimum Lorentz factor required

to avoid high pair-production optical depth that would inhibit the gamma-ray emission (i.e., $\tau_{\gamma\gamma} \leq 1$) for the whole $[\tilde{L}_{\text{iso}}, z]$ parameter space of the HL-GRB and sGRB families considered in Sec. 4.1. The Lorentz factors Γ defined in this way are reported in Table 1. Note that $E_{\gamma,t}$ belongs to the upper tail of the observed photon energy spectrum and therefore it allows us to define an upper limit for the optical depth for pair production for the assigned GRB parameters. The $\tau_{\gamma\gamma} \leq 1$ condition does not apply to LL-GRBs as the average photon energy is lower than the pair production threshold (see Sec. 2). Variations of the expected diffuse neutrino background as a function of t_v and Γ will be discussed in Sec. 4.2.

The observed neutrino spectrum from a single source at redshift z is defined as

$$F_\nu(E_\nu) = \frac{(1+z)^3}{4\pi\Gamma d_L^2(z)} \left(\frac{dN_\nu}{dE'_\nu} \right), \quad (3.23)$$

with $E' = E(1+z)/\Gamma$ and $d_L(z)$ the luminosity distance [76] computed assuming a flat Λ CDM cosmology with $\Omega_m = 0.32$, $\Omega_\Lambda = 0.68$ and $H_0 = 67 \text{ km s}^{-1} \text{ Mpc}^{-1}$ for the Hubble constant [77]. The total ν_e and ν_μ neutrino spectra from pion decay at the source and without flavor oscillation are: $(dN_{\nu_e}/dE'_\nu)_{\text{inj},\pi} = (dN_\nu/dE'_\nu)_{\mu\pi}$ and $(dN_{\nu_\mu}/dE'_\nu)_{\text{inj},\pi} = (dN_\nu/dE'_\nu)_{\mu\pi} + (dN_\nu/dE'_\nu)_\pi$ and similarly for kaons. Note that no τ neutrinos are produced.

Neglecting flavor oscillations, Fig. 5 (top panel) shows the neutrino energy spectra coming from pion, kaon and muon decays as a function of the energy for a typical HL-GRB and normalized as in Eq. (3.23) for a source at $z = 1$. The neutrino spectrum coming from muon decay from pions (μ_π , dashed blue line) exhibits four breaks, the first one corresponds to the first energy break ($E_{\nu,b,\mu}$), the second is due to the radiative cooling ($E_{\nu,\mu,\text{rc}}$), the third to the adiabatic cooling of muons ($E_{\nu,\mu,\text{ac}}$) and the fourth occurs at the same energy of the second break of the pion spectrum (blue line) and it is indeed due to the radiative cooling of the parent pion ($E_{\nu,\pi,\text{rc}}$, see Fig. 2 for comparison). For kaons (magenta lines) only the first break energy is relevant, while the neutrino spectrum coming from muon decay from kaons (μ_K , magenta dashed line) is similar to the μ_π one. The bottom panel of Fig. 5 shows the resultant ν_e (in black) and ν_μ (in red) neutrino energy spectra from pion and kaon decays and as a function of the energy without flavor oscillations for a HL-GRB at $z = 1$. Note as the cutoff in the neutrino energy spectrum corresponding to the maximum proton energy appears for energies slightly larger than the ones studied here.

3.4 Neutrino flavor oscillations

While neutrinos travel to reach the Earth they are subject to flavor oscillations and therefore the observed flux will be (see e.g., Appendix B of [44]):

$$\left(\frac{dN_{\nu_\mu}}{dE'_\nu} \right)_{\text{osc}} = \left[\frac{1}{4} \sin^2(2\theta_\odot) \right] \left(\frac{dN_{\nu_e}}{dE'_\nu} \right)_{\text{inj}} + \frac{1}{8} [4 - \sin^2(2\theta_\odot)] \left(\frac{dN_{\nu_\mu}}{dE'_\nu} \right)_{\text{inj}}. \quad (3.24)$$

with $\sin^2(2\theta_\odot) \simeq 8/9$. Note that while ν_τ are not produced at the source, the three neutrino flavors are equally abundant after flavor oscillations.

Figure 6 shows the expected $E_\nu^2 F_{\text{osc}}^{\nu_\mu}$ (computed through Eqs. 3.23 and 3.24) as a function of the energy for a typical HL-GRB ($\tilde{L}_{\text{iso}} = 10^{52} \text{ erg s}^{-1}$, blue line), LL-GRB ($\tilde{L}_{\text{iso}} = 10^{48} \text{ erg s}^{-1}$, green line), and for a sGRB ($\tilde{L}_{\text{iso}} = 10^{51} \text{ erg s}^{-1}$, red line) located at $z = 1$ and including contributions from pion, kaon and muon decays. Note as the HL-GRBs give the highest flux as expected, while the LL-GRB and the sGRB neutrino spectra are two-three orders of magnitude smaller than the HL-GRB one for the adopted input parameters. Note

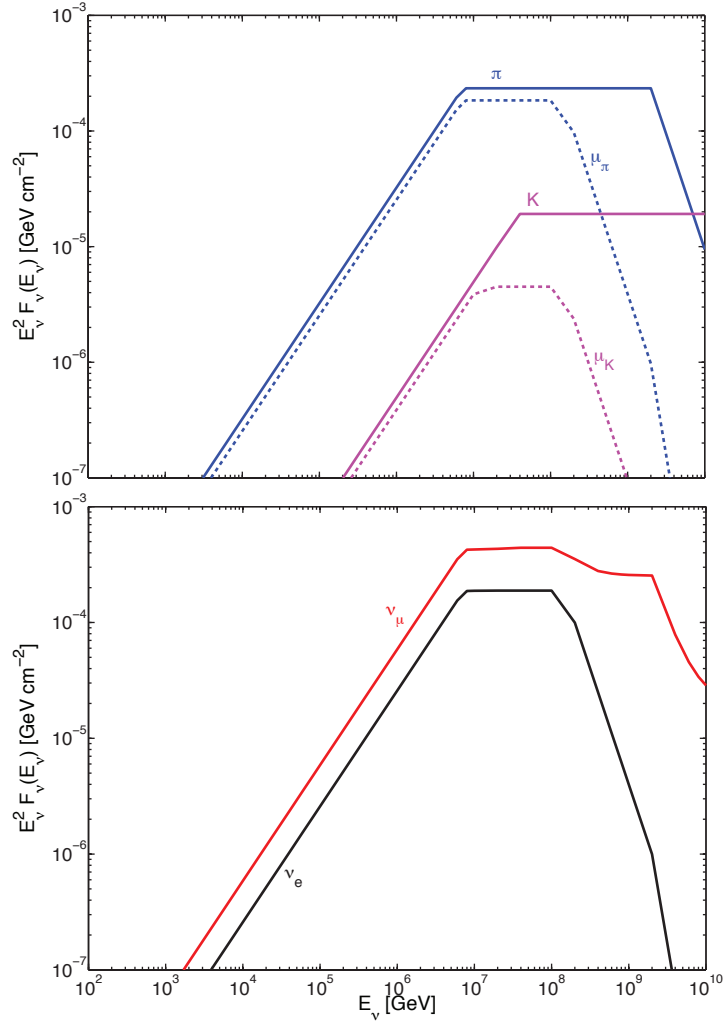


Figure 5. Predicted $E_\nu^2 F_\nu(E_\nu)$ for a typical HL-GRB ($\tilde{L}_{\text{iso}} = 10^{52} \text{ erg s}^{-1}$, $z = 1$) without flavor oscillations. Top: Neutrino fluence from π (blue line) and K (magenta line) decays as well as from μ from pion decay (μ_π , dashed blue line) and μ from kaon decay (μ_K , dashed magenta line). Bottom: $E_\nu^2 F_{\nu_e}(E_\nu)$ (black line) and $E_\nu^2 F_{\nu_\mu}(dE_\nu)$ (red line) for a typical HL-GRB and without flavor oscillations.

as by adopting the analytical prescription developed in Sec. 3, we find that our estimation of the neutrino flux from GRBs gave results close to the ones obtained adopting numerical routines in [10, 20, 74], by adopting their same GRB inputs.

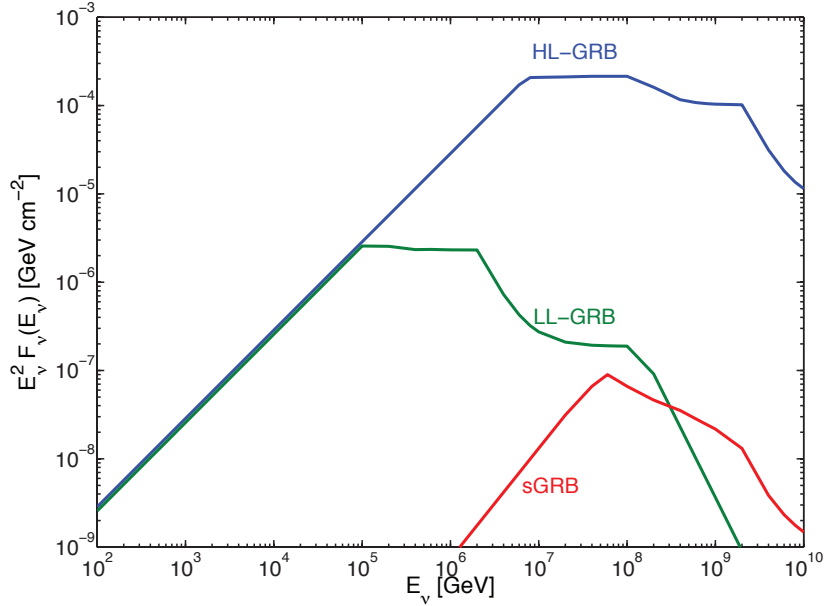


Figure 6. Predicted $E_\nu^2 F_\nu(E_\nu)$ for a typical HL-GRB ($\tilde{L}_{\text{iso}} = 10^{52}$ erg s $^{-1}$), LL-GRB ($\tilde{L}_{\text{iso}} = 10^{48}$ erg s $^{-1}$), and sGRB ($\tilde{L}_{\text{iso}} = 10^{51}$ erg s $^{-1}$) at $z = 1$ with flavor oscillations included. The HL-GRBs exhibit the highest flux and the kaon contribution affects the high-energy tail of the spectra in all cases.

4 High-energy diffuse neutrino background from gamma-ray bursts

In this section, we present our results on the high-energy diffuse neutrino background from GRB fireballs. We first discuss the expected neutrino background within the *canonical* model in terms of the astrophysical uncertainties on the local GRB rates and luminosity functions (see Table 1), then we study the dependence of the high-energy diffuse neutrino flux from the model parameters for each GRB family (see Table 2).

4.1 Expected diffuse background and uncertainties on the local rate and luminosity function of each GRB family

The diffuse neutrino intensity from each GRB component (X) can be defined in terms of the gamma-ray luminosity function, through $\Phi_X(\tilde{L}_{\text{iso}})d\tilde{L}_{\text{iso}} = \Phi_X(\tilde{L}_\nu)d\tilde{L}_\nu$ with Φ the LF introduced in Sec. 2 (normalized to unity after integration over luminosity):

$$I_X(E_\nu) = \int_{z_{\text{min}}}^{z_{\text{max}}} dz \int_{\tilde{L}_{\text{min}}}^{\tilde{L}_{\text{max}}} d\tilde{L}_{\text{iso}} \frac{c}{4\pi H_0 \Gamma} \frac{1}{\sqrt{\Omega_M(1+z)^3 + \Omega_\Lambda}} R_X(z) \Phi_X(\tilde{L}_{\text{iso}}) \left(\frac{dN_{\nu\mu}}{dE'_\nu} \right)_{\text{osc}} \quad (4.1)$$

In the numerical computation of the neutrino background, we assume $z_{\text{min}} = 0$ and $z_{\text{max}} = 11$, $\tilde{L}_{\text{iso}} \in [\tilde{L}_{\text{min}}, \tilde{L}_{\text{max}}]$ with \tilde{L}_{min} and \tilde{L}_{max} defined as in Table 1 for each family X, and $E'_\nu = E_\nu(1+z)/\Gamma$. Note as the chosen values for t_ν and Γ (Table 1) should guarantee us to extrapolate an average description of the whole GRB population. However, our estimation of the diffuse neutrino emission from GRBs also depends on parameters such as ϵ_e , ϵ_B , Γ and $h_{\gamma p}$ that are currently poorly constrained from observations (see discussion in Sec. 4.2) and should therefore be considered with caution.

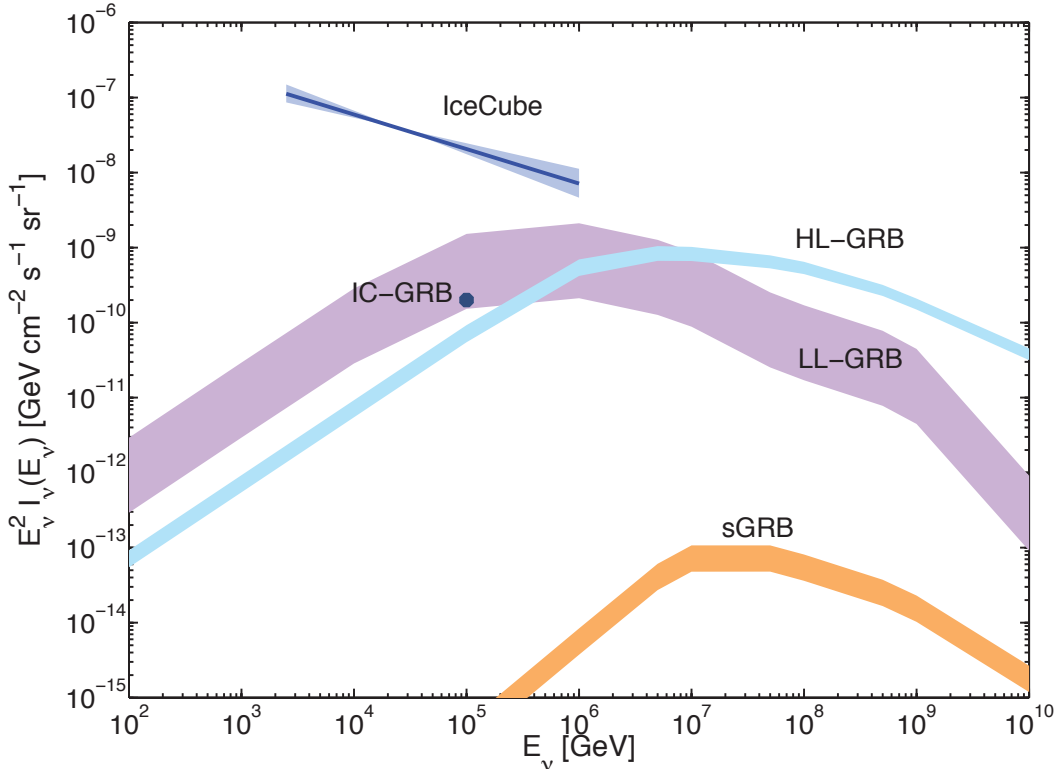


Figure 7. Diffuse ν_μ intensity as a function of the neutrino energy after flavor oscillations for the HL-GRB (blue band), LL-GRB (violet band) and sGRB (orange band) families. The bands represent uncertainties related to the luminosity functions and local rates (Table 1), whereas all the other GRB parameters are fixed to the *canonical* values. The best fit estimation of the high-energy diffuse neutrino flux as in [43] is plotted in light blue, while the blue dot (IC-GRB) marks the upper limit of the GRB diffuse neutrino flux from the IceCube Collaboration [20]. The diffuse neutrino background from GRB fireballs is smaller than the observed high-energy IceCube neutrino flux in the sub-PeV energy range and it scales differently as a function of the neutrino energy.

For each population X, we implement the analytical recipe described in Sec. 3 and automatically define the neutrino energy spectrum according to the specific hierarchy among the different cooling processes for each $(\tilde{L}_{\text{iso}}, z)$. Note as for luminosities and redshifts different than the ones adopted in Figs. 2, 3 and 4, the hierarchy among the cooling times changes. For example, we find that the adiabatic cooling becomes relevant for pions and kaons when \tilde{L}_{iso} is on the lower tail of the studied luminosity interval for all the three GRB families.

We do not include HL-GRBs and sGRBs whose parameters $(\tilde{L}_{\text{iso}}, z)$ violate the condition $\tau_{\gamma\gamma} \leq 1$ (Eq. 3.22) in our calculations. However, for the assumed input parameters, $\tau_{\gamma\gamma} > 1$ is realized only for sources with $z > 7$ and with luminosities at the upper extreme of their interval. Therefore, our computation might underestimate the expected diffuse flux only by a few % since the diffuse neutrino flux is not affected from sources at $z > 7$.

Figure 7 shows the diffuse high-energy neutrino intensity for the HL-GRB (light-blue band), LL-GRB (violet band) and sGRB (orange band) components as a function of the neutrino energy. Each band takes into account the uncertainty due to the LF determination as from Table 1.

Our results should be compared with the recent IceCube discovery of high-energy neutrinos [43] (blue line in Fig. 7), whose sources are still unknown as well as with the unsuccessful searches on GRBs from the IceCube telescope [16–20]. The total estimated diffuse flux from the GRB prompt emission can be as large as $2 \times 10^{-9} \text{ GeV cm}^{-2} \text{ s}^{-1} \text{ sr}^{-1}$ at 10^6 GeV and it is therefore slightly lower than the best fit of the high-energy neutrino flux detected with IceCube (blue line in Fig. 7) between 25 TeV and 1.4 PeV. Our estimated total diffuse emission is smaller than the IceCube flux at lower energies and it scales differently as a function of the neutrino energy. This implies that, assuming that the fireball model properly describes the GRB neutrino emission, GRBs cannot be the major contributors to the observed IceCube flux for the sub-PeV region.

IceCube results based on the monitoring of 505 observed GRBs are presented in [20] with four years of data. Extrapolating from the high-energy neutrino flux recently detected, it is estimated in [20] that the GRB diffuse emission at 100 TeV should be smaller than $2 \times 10^{-10} \text{ GeV cm}^{-2} \text{ s}^{-1} \text{ sr}^{-1}$ (blue dot in Fig. 7, IC-GRB). Although it might be that such extrapolation on the GRB emission underestimates the real GRB diffuse flux, as IceCube is sensitive to the first break energy that occurs for $E_\nu > 100 \text{ TeV}$ (see Fig. 6), such upper bound is very close to our results for the HL-GRB family. In fact our estimated high-energy neutrino intensity at $E_\nu = 100 \text{ TeV}$ is $8 \times 10^{-11} \text{ GeV cm}^{-2} \text{ s}^{-1} \text{ sr}^{-1}$ for HL-GRBs. Comparing the contribution from the HL-GRB component with the exclusion limits presented in Fig. 1 of [20], we conclude that our results are compatible with current observations and in rough agreement with the updated computation of the Waxman-Bahcall flux [8] proposed by the IceCube Collaboration (see Fig. 1 of Ref. [20]). Rescaling the HL-GRB flux in Fig. 6 to the proton-to-photon luminosity ratio adopted by the IceCube Collaboration ($h_{p\gamma} = 0.1$), at $5 \times 10^6 \text{ GeV}$, our predicted stacking flux for 505 sources is $9 \times 10^{-3} \text{ GeV cm}^{-2}$, which is roughly in agreement with the prediction presented in Fig. 2 of [20] for the standard GRB model.³

The total expected neutrino emission from GRBs might be further enhanced by GRBs that do not trigger the detector because of their low flux or because they are dark in gamma-rays [23, 70, 78]. However, such contribution is not discussed in this work. We also estimated that the contribution from pp interactions should be subleading with respect to the one from $p\gamma$ interactions in the energy range of relevance. We expect that the overall normalization of the expected neutrino background from GRBs should be independent from the employed GRB model for fixed GRB parameters (see, e.g. Fig. 1 of [15]), although peaking in slightly different energy intervals.

4.2 Expected diffuse background and uncertainties on the jet parameters

Up to now, we relied on the *canonical* models for each GRB family. In this Section, we adopt the GRB luminosity functions and local rates corresponding to the upper limits of the expected diffuse backgrounds plotted in Fig. 7 and discuss how our estimation depends on the photon-to-proton luminosity ratio $h_{\gamma p}$, the bulk Lorentz factor Γ and the variability time t_v .

- *Dependence on the photon-to-proton luminosity ratio $h_{\gamma p}$.* In our canonical model we assumed $h_{\gamma p} = 10^{-2}$ for the HL-GRB and the sGRB components. Such a choice is

³Note that we focus on the HL-GRB family in the comparison with the IceCube results on stacking searches as those are the sources for which there is higher probability to have a photon-neutrino correlation adopted in the IceCube procedure for the GRB discrimination.

Table 2. Variability range of the GRB model parameters adopted in the estimation of the diffuse high-energy neutrino flux. The variability time t_v is expressed in s.

	Γ_{\min}	Γ	Γ_{\max}	$t_{v,\min}$	t_v	$t_{v,\max}$
HL-GRB	100	500	1000	10^{-3}	0.1	1
LL-GRB	2	5	20	10	100	200
sGRB	100	650	1000	10^{-3}	10^{-2}	0.05

consistent with a coherent picture of neutrinos, gamma-rays and cosmic rays assuming that GRBs are main sources of the observed UHECR flux (see, e.g., [10, 28–30] for dedicated discussions). Current data suggest lower bounds for this parameter, but its precise value has not yet been fixed. Variations of $h_{\gamma p}$ correspond to an energy-independent scaling of the neutrino flux shown in Fig. 7 as from Eq. (3.20).

Assuming that the cosmic ray energy budget of the HL-GRB and LL-GRB populations are comparable, $h_{\gamma p}$ for the LL-GRB component should be roughly three orders of magnitude smaller than the HL-GRB one (because of the difference in \tilde{L}_{iso} of the two populations). However, $h_{\gamma p} = 10^{-5}$ would give a diffuse neutrino flux above the current IceCube observed flux. We therefore chose our canonical value in such a way to boost the neutrino emission with respect to the photon one without violating the IceCube current bounds [43]. We stress, however, that this parameter is currently unconstrained and scalings of the LL-GRB intensity with respect to the one presented here are not excluded yet. See also discussions in Refs. [25, 34, 39, 75].

- *Dependence on the bulk Lorentz factor Γ .* As mentioned in Sec. 3.3, we fixed t_v of each GRB family to the observed values in the *canonical* model and determined Γ to guarantee optically thin GRBs for the whole $(\tilde{L}_{\text{iso}}, z)$ parameter space. Here, we loosen the $\tau_{\gamma\gamma} \leq 1$ constraint and study how the diffuse emission of each GRB family varies as a function of Γ . For the HL-GRB and sGRB components, we define Γ_{\min} and Γ_{\max} inspired from *Fermi* data [75, 79, 80], as reported in Table 2. The Γ factor of LL-GRBs is poorly constrained due to the scarce statistics collected on these sources up to now. However, Γ of a few seems to be favored (see, e.g., [75, 81] and references therein). We therefore consider $\Gamma_{\min} = 2$ and $\Gamma_{\max} = 20$. The adopted intervals in Γ for each GRB family are summarised in Table 2.

Figure 8 (top panel) shows the correspondent diffuse GRB intensity as a function of the Γ parameter. In general, the expected diffuse neutrino intensity increases as Γ decreases. Besides the intensity normalization, Γ also affects the neutrino break energies as from Sec. 3. Note that, by adopting a wide range of variability for the HL-GRB component, the diffuse intensity could even be comparable with the IceCube high-energy neutrino flux. However, an average $\Gamma = 100$ for the HL-GRB population does not guarantee optically thin sources for any \tilde{L}_{iso} and z , besides being disfavored from the most recent IceCube results [20].

- *Dependence on the variability time t_v .* The variability time t_v has been fixed in the *canonical* model to the average value preferred from observations [23, 64, 75]. Here, we study how the diffuse intensity changes for a minimum variability time $t_{v,\min}$ and

a maximum one ($t_{v,\max}$) defined in Table 2 as suggested from recent data [23, 64, 75]. Note that we consider $t_{v,\min}$ one order of magnitude smaller than the one defined for example in Fig. 4 of Ref. [64] assuming that current experimental sensitivity might not allow to detect even smaller variability times.

Figure 8 (bottom panel) shows the correspondent diffuse GRB intensity as a function of the variability time t_v . Similarly to Γ , the variability time affects the normalization and the neutrino break energies as from Sec. 3.

In all the studied scenarios, GRBs cannot explain the total detected high-energy IceCube neutrino flux in the sub-PeV energy range. However, for certain choices of the model parameters, the diffuse neutrino emission from GRBs can reach the IceCube band around PeV energies.

5 Discussion and conclusions

Gamma-ray bursts (GRBs) are considered to be high-energy neutrino emitters and candidate sources of the ultra-high energy cosmic rays. We elaborate an analytical model to compute the neutrino flux from GRBs based on the fireball picture, by including the pion, kaon and muon decay contributions and taking into account radiative, adiabatic and hadronic cooling processes.

We revisited the fireball model for the GRB neutrino emission [8, 10], providing a simple analytical recipe to compute the GRB neutrino flux. For the first time, we included the kaon and muon contribution other than the pion one and discussed the role of adiabatic, hadronic and radiative coolings. Moreover, for the first time, we investigated the relevant cooling processes for different GRB families, i.e., long- (divided in low-luminosity and high-luminosity) and short-duration bursts and conclude that while the hadronic cooling is negligible for the HL-GRB and sGRB families, the radiative cooling is always relevant, and the adiabatic one is not negligible for muons, and for pions of LL-GRBs and sGRBs.

By adopting up-to-date luminosity functions corrected for beaming effects, we extrapolated the expected diffuse neutrino flux from the long- (divided in low- and high-luminosity) and short duration bursts. Assuming that each burst has typical parameters inferred from observations and luminosity varying with the redshift as prescribed from the luminosity functions in Sec. 2, we found that the estimated diffuse background intensity could be as large as $2 \times 10^{-9} \text{ GeV cm}^{-2} \text{ s}^{-1} \text{ sr}^{-1}$. The low-luminosity GRBs, being the most abundant ones, seem to dominate the overall diffuse intensity in the sub-PeV region, while high-luminosity GRBs are the major source at larger energies. Such conclusions are also supported from variations of the model parameters within the range allowed from observations. We conclude that GRBs do not appear to be the leading sources originating the observed IceCube neutrino flux in the sub-PeV region, if the latter is interpreted in terms of unresolved sources. Very recently, the possibility that the PeV neutrinos originate by GRB cosmic rays interacting with the interstellar gas while propagating in the host galaxy has also been investigated [35]. However, also such an estimation appears to predict an insufficient neutrino flux.

Previous estimates of the diffuse neutrino emission from the high-luminosity GRBs [22, 24, 33] found a total diffuse flux from GRBs of the order of $10^{-8} \text{ GeV cm}^{-2} \text{ s}^{-1} \text{ sr}^{-1}$ depending on the luminosity function and redshift evolution adopted. Our results are in agreement with the more conservative ones presented in Ref. [32], where an analysis on triggered and un-triggered sources has been conducted, normalizing the triggered GRBs through the ones

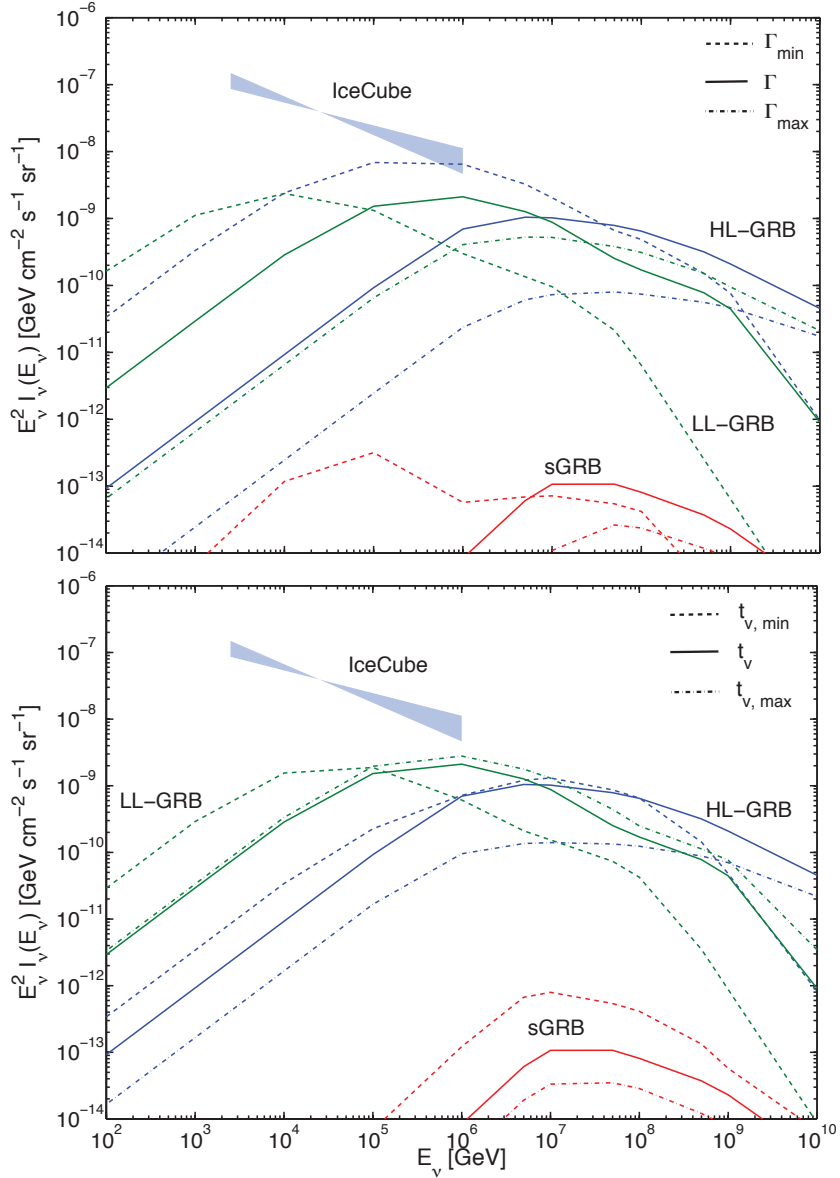


Figure 8. Diffuse ν_μ intensity as a function of the neutrino energy after flavor oscillations for the HL-GRB (blue), LL-GRB (green) and sGRB (red) families, for different values of Γ (top panel) and t_v (bottom panel) as from Table 2. The best fit estimation of the high-energy diffuse neutrino flux as in [43] is plotted in light blue.

detected with *Fermi*/GBM. In agreement with Refs. [24, 25], we conclude that the neutrino flux from the low-luminosity GRBs could be comparable to the one from the high-luminosity GRBs and such GRBs could be the main contributors to the IceCube high-energy neutrino flux around $E_\nu \sim \text{PeV}$.

Our results, although should be considered with caution given the uncertainties on the GRB models for the neutrino emission and their parameters, suggest that larger exposure is required to discriminate neutrinos from high-luminosity GRBs in forthcoming stacking

searches. Moreover, we find that the GRBs do not appear to be the main sources of the sub-PeV neutrino flux observed by IceCube. However, if the high-energy diffuse neutrino flux results from the superposition of several unresolved sources, for example comparing the contribution from starburst galaxies (see Fig. 4 of [82]) with the one from high-luminosity and low luminosity GRBs, it appears that while starbursts could explain the low-energy tail of the IceCube flux up to 0.5 PeV, the GRBs could be responsible for the high-energy tail of the neutrino spectrum, if this has a cutoff at energies larger than a few PeV. Such a hypothesis could be eventually tested in the coming years in light of the increasing IceCube statistics.

Acknowledgments

We are grateful to Thomas Janka, Kohta Murase, Elisa Resconi, Mike Richman, Eli Waxman, and Ralph Wijers for useful discussions. This work was supported by the Netherlands Organization for Scientific Research (NWO) through a Vidi grant.

References

- [1] P. Kumar and B. Zhang, “The Physics of Gamma-Ray Bursts and Relativistic Jets,” *Phys. Rept.* **561** (2014) 1 [arXiv:1410.0679 [astro-ph.HE]].
- [2] P. Mészáros, “Gamma-Ray Bursts,” *Rept. Prog. Phys.* **69** (2006) 2259 [astro-ph/0605208].
- [3] E. Waxman, “Cosmological gamma-ray bursts and the highest energy cosmic rays,” *Phys. Rev. Lett.* **75** (1995) 386 [astro-ph/9505082].
- [4] M. Vietri, “On the acceleration of ultrahigh-energy cosmic rays in gamma-ray bursts,” *Astrophys. J.* **453** (1995) 883 [astro-ph/9506081].
- [5] C. Kouveliotou *et al.*, “Identification of two classes of gamma-ray bursts,” *Astrophys. J.* **413** (1993) L101.
- [6] S. E. Woosley, “Gamma-ray bursts from stellar mass accretion disks around black holes,” *Astrophys. J.* **405** (1993) 273.
- [7] D. Eichler, M. Livio, T. Piran and D. N. Schramm, “Nucleosynthesis, Neutrino Bursts and Gamma-Rays from Coalescing Neutron Stars,” *Nature* **340** (1989) 126.
- [8] E. Waxman and J. N. Bahcall, “High-energy neutrinos from cosmological gamma-ray burst fireballs,” *Phys. Rev. Lett.* **78** (1997) 2292 [astro-ph/9701231].
- [9] E. Waxman, “Gamma-ray bursts: The Underlying model,” *Lect. Notes Phys.* **598** (2003) 393 [astro-ph/0303517].
- [10] S. Hümmer, P. Baerwald and W. Winter, “Neutrino Emission from Gamma-Ray Burst Fireballs, Revised,” *Phys. Rev. Lett.* **108** (2012) 231101 [arXiv:1112.1076 [astro-ph.HE]].
- [11] A. Shemi and T. Piran, “The appearance of cosmic fireballs,” *Astrophys. J.* **365** (1990) L55.
- [12] M. J. Rees and P. Mészáros, “Relativistic fireballs – energy conversion and time - scales,” *Mon. Not. Roy. Astron. Soc.* **258** (1992) 41.
- [13] M. J. Rees and P. Mészáros, “Dissipative photosphere models of gamma-ray bursts and x-ray flashes,” *Astrophys. J.* **628** (2005) 847 [astro-ph/0412702].
- [14] B. Zhang and H. Yan, “The Internal-Collision-Induced Magnetic Reconnection and Turbulence (ICMART) Model of Gamma-Ray Bursts,” *Astrophys. J.* **726** (2011) 90 [arXiv:1011.1197 [astro-ph.HE]].
- [15] B. Zhang and P. Kumar, “Model-dependent high-energy neutrino flux from Gamma-Ray Bursts,” *Phys. Rev. Lett.* **110** (2013) 12, 121101 [arXiv:1210.0647 [astro-ph.HE]].

- [16] R. Abbasi *et al.* [IceCube Collaboration], “Search for muon neutrinos from Gamma-Ray Bursts with the IceCube neutrino telescope,” *Astrophys. J.* **710** (2010) 346 [arXiv:0907.2227 [astro-ph.HE]].
- [17] R. Abbasi *et al.* [IceCube Collaboration], “Limits on Neutrino Emission from Gamma-Ray Bursts with the 40 String IceCube Detector,” *Phys. Rev. Lett.* **106** (2011) 141101 [arXiv:1101.1448 [astro-ph.HE]].
- [18] R. Abbasi *et al.* [IceCube Collaboration], “An absence of neutrinos associated with cosmic-ray acceleration in γ -ray bursts,” *Nature* **484** (2012) 351 [arXiv:1204.4219 [astro-ph.HE]].
- [19] M. G. Aartsen *et al.* [The IceCube Collaboration], “The IceCube Neutrino Observatory Part I: Point Source Searches,” Proceedings of the 33rd conference in the ICRC series (2–9 July 2013, Rio de Janeiro, Brazil), arXiv:1309.6979 [astro-ph.HE].
- [20] M. G. Aartsen *et al.* [IceCube Collaboration], “Search for Prompt Neutrino Emission from Gamma-Ray Bursts with IceCube,” *Astrophys. J.* **805** (2015) 1, L5 [arXiv:1412.6510 [astro-ph.HE]].
- [21] P. Baerwald, S. Hümmer and W. Winter, “Systematics in the Interpretation of Aggregated Neutrino Flux Limits and Flavor Ratios from Gamma-Ray Bursts,” *Astropart. Phys.* **35** (2012) 508 [arXiv:1107.5583 [astro-ph.HE]].
- [22] H. N. He *et al.*, *Astrophys. J.* **752** (2012) 29 [arXiv:1204.0857 [astro-ph.HE]].
- [23] R. Y. Liu, X. Y. Wang and Z. G. Dai, “Nearby low-luminosity GRBs as the sources of ultra-high energy cosmic rays revisited,” *Mon. Not. Roy. Astron. Soc.* **418** (2011) 1382 [arXiv:1108.1551 [astro-ph.HE]].
- [24] N. Gupta and B. Zhang, “Neutrino Spectra from Low and High Luminosity Populations of Gamma Ray Bursts,” *Astropart. Phys.* **27** (2007) 386 [astro-ph/0606744].
- [25] K. Murase, K. Ioka, S. Nagataki and T. Nakamura, “High Energy Neutrinos and Cosmic-Rays from Low-Luminosity Gamma-Ray Bursts?,” *Astrophys. J.* **651** (2006) L5 [astro-ph/0607104].
- [26] K. Murase and S. Nagataki, “High energy neutrino emission and neutrino background from gamma-ray bursts in the internal shock model,” *Phys. Rev. D* **73** (2006) 063002 [astro-ph/0512275].
- [27] E. Waxman and J. N. Bahcall, “High-energy neutrinos from astrophysical sources: An Upper bound,” *Phys. Rev. D* **59** (1999) 023002 [hep-ph/9807282].
- [28] K. Asano and P. Mészáros, “Neutrino and Cosmic-Ray Release from Gamma-Ray Bursts: Time-Dependent Simulations,” *Astrophys. J.* **785** (2014) 54 [arXiv:1402.6057 [astro-ph.HE]].
- [29] M. Ahlers, M. C. Gonzalez-Garcia and F. Halzen, “GRBs on probation: testing the UHE CR paradigm with IceCube,” *Astropart. Phys.* **35** (2011) 87 [arXiv:1103.3421 [astro-ph.HE]].
- [30] P. Baerwald, M. Bustamante and W. Winter, “Are gamma-ray bursts the sources of ultra-high energy cosmic rays?,” *Astropart. Phys.* **62** (2015) 66 [arXiv:1401.1820 [astro-ph.HE]].
- [31] M. Bustamante, P. Baerwald, K. Murase and W. Winter, “Neutrino and cosmic-ray emission from multiple internal shocks in gamma-ray bursts,” *Nat. Commun.* **6**, 6783 (2015) [arXiv:1409.2874 [astro-ph.HE]].
- [32] R. Y. Liu and X. Y. Wang, “Diffuse PeV neutrinos from gamma-ray bursts,” *Astrophys. J.* **766** (2013) 73 [arXiv:1212.1260 [astro-ph.HE]].
- [33] I. Cholis and D. Hooper, “On The Origin of IceCube’s PeV Neutrinos,” *JCAP* **1306** (2013) 030 [arXiv:1211.1974 [astro-ph.HE]].
- [34] K. Murase and K. Ioka, “TeV–PeV Neutrinos from Low-Power Gamma-Ray Burst Jets inside Stars,” *Phys. Rev. Lett.* **111** (2013) 12, 121102 [arXiv:1306.2274 [astro-ph.HE]].

- [35] Z. Y. Wang, X. Y. Wang and J. F. Wang, “Neutrinos from gamma-ray bursts: propagation of cosmic rays in their host galaxies,” *Astrophys. J.* **803** (2015) 1, L5 [arXiv:1503.04932 [astro-ph.HE]].
- [36] S. Razzaque and L. Yang, “PeV-EeV neutrinos from GRB blast waves in IceCube and future neutrino telescopes,” *Phys. Rev. D* **91** (2015) 043003 [arXiv:1411.7491 [astro-ph.HE]].
- [37] S. Razzaque, “Long-lived PeVeV neutrinos from gamma-ray burst blastwave,” *Phys. Rev. D* **88** (2013) 10, 103003 [arXiv:1307.7596 [astro-ph.HE]].
- [38] M. Petropoulou, D. Giannios and S. Dimitrakoudis, “Implications of a PeV neutrino spectral cut-off in gamma-ray burst models,” *Mon. Not. Roy. Astron. Soc.* **445** (2014) 1, 570 [arXiv:1405.2091 [astro-ph.HE]].
- [39] E. Nakar, “A unified picture for low-luminosity and long gamma-ray bursts based on the extended progenitor of llgrb 060218/SN 2006aj,” *Astrophys. J.* **807** (2015) 172 [arXiv:1503.00441 [astro-ph.HE]].
- [40] M. G. Aartsen *et al.* [IceCube Collaboration], “First observation of PeV-energy neutrinos with IceCube,” *Phys. Rev. Lett.* **111** (2013) 021103 [arXiv:1304.5356 [astro-ph.HE]].
- [41] M. G. Aartsen *et al.* [IceCube Collaboration], “Evidence for High-Energy Extraterrestrial Neutrinos at the IceCube Detector,” *Science* **342** (2013) 1242856 [arXiv:1311.5238 [astro-ph.HE]].
- [42] M. G. Aartsen *et al.* [IceCube Collaboration], “Observation of High-Energy Astrophysical Neutrinos in Three Years of IceCube Data,” *Phys. Rev. Lett.* **113** (2014) 101101 [arXiv:1405.5303 [astro-ph.HE]].
- [43] M. G. Aartsen *et al.* [IceCube Collaboration], “Atmospheric and Astrophysical Neutrinos above 1 TeV Interacting in IceCube,” *Phys. Rev. D* **91** (2015) 022001 [arXiv:1410.1749 [astro-ph.HE]].
- [44] L. A. Anchordoqui *et al.*, “Cosmic Neutrino Pevatrons: A Brand New Pathway to Astronomy, Astrophysics, and Particle Physics,” *JHEAp* **1-2** (2014) 1 [arXiv:1312.6587 [astro-ph.HE]].
- [45] D. Wanderman and T. Piran, “The luminosity function and the rate of Swift’s Gamma Ray Bursts,” *Mon. Not. Roy. Astron. Soc.* **406** (2010) 1944 [arXiv:0912.0709 [astro-ph.HE]].
- [46] J. J. Wei *et al.*, “Cosmological Tests Using GRBs, the Star Formation Rate and Possible Abundance Evolution,” *Mon. Not. Roy. Astron. Soc.* **439** (2014) 3329 [arXiv:1306.4415 [astro-ph.HE]].
- [47] E. J. Howell *et al.*, “Constraining the rate and luminosity function of Swift gamma-ray bursts,” *Mon. Not. Roy. Astron. Soc.* **444** (2014) 15 [arXiv:1407.2333 [astro-ph.HE]].
- [48] E. Liang, B. Zhang and Z. G. Dai, “Low Luminosity Gamma-Ray Bursts as a Unique Population: Luminosity Function, Local Rate, and Beaming Factor,” *Astrophys. J.* **662** (2007) 1111 [astro-ph/0605200].
- [49] O. Bromberg, E. Nakar and T. Piran, “Are low luminosity GRBs generated by relativistic jets?,” *Astrophys. J.* **739** (2011) L55 [arXiv:1107.1346 [astro-ph.HE]].
- [50] H. Yuksel, M. D. Kistler, J. F. Beacom and A. M. Hopkins, “Revealing the High-Redshift Star Formation Rate with Gamma-Ray Bursts,” *Astrophys. J.* **683** (2008) L5 [arXiv:0804.4008 [astro-ph]].
- [51] T. Dahlen *et al.*, “High redshift supernova rates,” *Astrophys. J.* **613** (2004) 189 [astro-ph/0406547].
- [52] X. Dai, “Intensity Distribution and Luminosity Function of the Swift Gamma-Ray Bursts,” *Astrophys. J.* **697** (2009) L68 [arXiv:0812.4466 [astro-ph]].
- [53] D. Band *et al.* “BATSE observations of gamma-ray burst spectra. 1. Spectral diversity,” *Astrophys. J.* **413** (1993) 281.

- [54] L. Amati *et al.*, “Intrinsic spectra and energetics of BeppoSAX gamma-ray bursts with known redshifts,” *Astron. Astrophys.* **390** (2002) 81 [astro-ph/0205230].
- [55] G. Ghirlanda, G. Ghisellini and C. Firmani, “Probing the existence of the E(peak) - E(iso) correlation in long gamma ray bursts,” *Mon. Not. Roy. Astron. Soc.* **361** (2005) L10 [astro-ph/0502186].
- [56] D. Yonetoku *et al.*, “Gamma-ray burst formation rates inferred from the spectral peak energy-peak luminosity relation,” *Astrophys. J.* **609** (2004) 935 [astro-ph/0309217].
- [57] G. Ghirlanda *et al.*, “Gamma Ray Bursts in the comoving frame,” *Mon. Not. Roy. Astron. Soc.* **420** (2012) 483 [arXiv:1107.4096 [astro-ph.HE]].
- [58] D. Guetta and M. Della Valle, “On the Rates of Gamma Ray Bursts and Type Ib/c Supernovae,” *Astrophys. J.* **657** (2007) L73 [astro-ph/0612194].
- [59] R. Narayan, B. Paczynski and T. Piran, “Gamma-ray bursts as the death throes of massive binary stars,” *Astrophys. J.* **395** (1992) L83 [astro-ph/9204001].
- [60] S. Ando, “Short gamma-ray bursts as a possible probe of binary neutron star mergers,” *JCAP* **0406** (2004) 007 [astro-ph/0405411].
- [61] D. Wanderman and T. Piran, “The rate, luminosity function and time delay of non-Collapsar short GRBs,” *Mon. Not. Roy. Astron. Soc.* **448** (2015) 4, 3026 [arXiv:1405.5878 [astro-ph.HE]].
- [62] L. Nava, G. Ghirlanda, G. Ghisellini and A. Celotti, “Spectral properties of 438 GRBs detected by Fermi/GBM,” *Astron. Astrophys.* **530** (2011) A21 [arXiv:1012.2863 [astro-ph.HE]].
- [63] A. Shahmoradi and R. J. Nemiroff, “Short vs. Long Gamma-Ray Bursts: A Comprehensive Study of Energetics and Prompt Gamma-Ray Correlations,” *Mon. Not. Roy. Astron. Soc.* **451** (2015) 4645 [arXiv:1412.5630 [astro-ph.HE]].
- [64] G. A. MacLachlan *et al.*, “Minimum Variability Time Scales of Long and Short GRBs,” *Mon. Not. Roy. Astron. Soc.* **432** (2013) 857 [arXiv:1201.4431 [astro-ph.HE]].
- [65] P. Baerwald, S. Hümmer and W. Winter, “Magnetic Field and Flavor Effects on the Gamma-Ray Burst Neutrino Flux,” *Phys. Rev. D* **83** (2011) 067303 [arXiv:1009.4010 [astro-ph.HE]].
- [66] D. Guetta *et al.*, “Neutrinos from individual gamma-ray bursts in the BATSE catalog,” *Astropart. Phys.* **20** (2004) 429 [astro-ph/0302524].
- [67] S. Eidelman *et al.* [Particle Data Group Collaboration], “Review of particle physics. Particle Data Group,” *Phys. Lett. B* **592** (2004) 1.
- [68] A. E. Brenner *et al.*, “Experimental study of single-particle inclusive hadron scattering and associated multiplicities,” *Phys. Rev. D* **26** (1982) 1497.
- [69] J. Kakuwa *et al.*, “Prospects for Detecting Gamma-Ray Bursts at Very High Energies with the Cherenkov Telescope Array,” *Mon. Not. Roy. Astron. Soc.* **425** (2012) 514 [arXiv:1112.5940 [astro-ph.HE]].
- [70] S. Ando and J. F. Beacom, “Revealing the supernova-gamma-ray burst connection with TeV neutrinos,” *Phys. Rev. Lett.* **95** (2005) 061103 [astro-ph/0502521].
- [71] K. Asano and S. Nagataki, “Very high energy neutrinos originating from kaons in gamma-ray bursts,” *Astrophys. J.* **640** (2006) L9 [astro-ph/0603107].
- [72] Z. Li, “Note on the Normalization of Predicted GRB Neutrino Flux,” *Phys. Rev. D* **85** (2012) 027301 [arXiv:1112.2240 [astro-ph.HE]].
- [73] S. R. Kelner and F. A. Aharonian, “Energy spectra of gamma-rays, electrons and neutrinos produced at interactions of relativistic protons with low energy radiation,” *Phys. Rev. D* **78** (2008) 034013 [Erratum-ibid. *D* **82** (2010) 099901] [arXiv:0803.0688 [astro-ph]].

- [74] A. Mücke *et al.*, “SOPHIA: Monte Carlo simulations of photohadronic processes in astrophysics,” *Comput. Phys. Commun.* **124** (2000) 290 [astro-ph/9903478].
- [75] C. D. Dermer, K. Murase and Y. Inoue, “Photopion Production in Black-Hole Jets and Flat-Spectrum Radio Quasars as PeV Neutrino Sources,” *JHEAp* **3-4** (2014) 29 [arXiv:1406.2633 [astro-ph.HE]].
- [76] D. W. Hogg, “Distance measures in cosmology,” astro-ph/9905116.
- [77] P. A. R. Ade *et al.* [Planck Collaboration], “Planck 2013 results. XVI. Cosmological parameters,” *Astron. Astrophys.* **571** (2014) A16 [arXiv:1303.5076 [astro-ph.CO]].
- [78] S. Razzaque, P. Mészáros and E. Waxman, “TeV neutrinos from core collapse supernovae and hypernovae,” *Phys. Rev. Lett.* **93** (2004) 181101 [Erratum-*ibid.* **94** (2005) 109903] [astro-ph/0407064].
- [79] M. Ackermann *et al.* [Fermi Collaboration], “Detection of a spectral break in the extra hard component of GRB 090926A,” *Astrophys. J.* **729** (2011) 114 [arXiv:1101.2082 [astro-ph.HE]].
- [80] S. B. Cenko *et al.*, “Afterglow Observations of Fermi-LAT Gamma-Ray Bursts and the Emerging Class of Hyper-Energetic Events,” *Astrophys. J.* **732** (2011) 29 [arXiv:1004.2900 [astro-ph.HE]].
- [81] K. Toma, K. Ioka, T. Sakamoto and T. Nakamura, “Low-Luminosity GRB 060218: A Collapsar Jet from a Neutron Star, Leaving a Magnetar as a Remnant?,” *Astrophys. J.* **659** (2007) 1420 [astro-ph/0610867].
- [82] I. Tamborra, S. Ando and K. Murase, “Star-forming galaxies as the origin of diffuse high-energy backgrounds: Gamma-ray and neutrino connections, and implications for starburst history,” *JCAP* **1409** (2014) 09, 043 [arXiv:1404.1189 [astro-ph.HE]].